30B, 185 (1969); A. C. Irving, A. D. Martin, and C. Michael, Nucl. Phys. B32, 1 (1971); R. D. Field, Phys. Rev. D 5, 86 (1972).

[45]C. Chiu, in Proceedings of the Workshop on Particle Physics at Intermediate Energies, edited by R. D. Field [Lawrence Berkeley Laboratory Report No. UCRL-20655 (unpublished)]; R. C. Johnson, Phys. Letters 38B, 325 (1972).

[46]In the forward direction ($\theta_s = 0°$) the t-channel scattering angle is $\theta_t = \pi$ and the crossing angles are $\chi_1 = \pi$, $\chi_2 = 0$, $\chi_3 = 0$, thus from (2.34) we have $H_{\lambda_3\bar{\lambda}_1;\bar{\lambda}_4} = f_{\lambda_3\lambda_4;-\lambda_1}$.

[47]The convolution integral used to calculate the s-channel Pomeranchukon–Regge-pole cut ($P \cdot R$) amplitude receives its largest contributions from the small $|t|$ region of R because the Pomeranchukon amplitude P dies out rapidly with increasing $|t|$. Thus Regge amplitudes R that vanish or dip in the forward direction tend to give small $P \cdot R$ cut contributions.

[48]This is easily seen by examining the experimental values of ρ_{00}^J. This quantity is quite large for π exchange reactions ($\langle \rho_{00}^J \rangle = 0.7$), whereas for vector-meson production with $Y = 1$ exchange it is much smaller ($\langle \rho_{00}^J \rangle = 0.3$; see Fig. 4).

[49]The inclusion of a small K_B contribution as in our fits does not alter this conclusion.

[50]There is considerable evidence both phenomenological and theoretical that present-day cut models may indeed be wrong. See, for example, C. Lovelace, CERN Report No. CERN-TH-1359, 1971 (unpublished); J. W. Coleman and R. C. Johnson, Nucl. Phys. B33, 614 (1971). Also see Ref. 45.

[51]C. Michael and R. Odorico, Phys. Letters 34B, 422 (1971). These authors determined the s-channel helicity-nonflip and -flip F/D values to be $(F/D)_n^s = -2$ and $(F/D)_f^s = 0.27$, respectively, whereas we determined the t-channel helicity-nonflip and -flip F/D values to be $(F/D)_n^t = -4.3$ and $(F/D)_f^t = 0.14$, respectively. This makes a direct comparison somewhat difficult.

PHYSICAL REVIEW D VOLUME 6, NUMBER 7 1 OCTOBER 1972

Momentum Dependence of the 180° $\pi^- p$ Charge-Exchange Cross Section

V. Kistiakowsky, B. T. Feld, F. A. Triantis,* and R. K. Yamamoto
Massachusetts Institute of Technology,† Cambridge, Massachusetts 02139

and

R. D. Klem, P. Marcato,‡ I. A. Pless,§ and I. Spirn
Argonne National Laboratory, Argonne, Illinois 60439

and

E. F. Anelli, C. N. DeMarzo, and A. Romano
Istituto di Fisica dell'Universita di Bari, Bari, Italy
and Istituto Nazionale di Fisica Nucleare, Sottosezione di Bari, Bari, Italy

and

D. G. Crabb, A. C. Meyers, III, and J. R. O'Fallon
Saint Louis University, Saint Louis, Missouri 61303

(Received 11 May 1972)

The $\pi^- + p \to \pi^0 + n$ differential cross section at 180° has been measured for 52 values of π^- momentum from 1.8 to 6.0 GeV/c using a constant-geometry detection system. The average statistical uncertainty is ~5% and the systematic uncertainty is ~10%. The details of the experiment and the data analysis are discussed. The data are compared with those of other experiments with which they are generally in agreement. One set of data disagrees with those presented here and a possible reason for this is discussed. A five-parameter fit of the predictions of a dual-resonance model to our data gave excellent agreement. The differential cross sections at 180° for $\pi^\pm p$ elastic scattering have been compiled and the moduli and relative phase of the $T = \frac{1}{2}$ and $T = \frac{3}{2}$ pion-nucleon s- and u-channel amplitudes ($|A_{1/2}|$, $|A_{3/2}|$, and $\cos\delta$) have a minimum at $\sqrt{u} = 0.4$ GeV/c and, in the s channel, a corresponding minimum at $\sqrt{s} = 2.2$ GeV/c.

I. INTRODUCTION

The differential cross sections for the pion charge-exchange reaction

$$\pi^- + p \to \pi^0 + n$$

at 0° and 180° are of special interest because most models predict their energy dependence with relatively few parameters and, in principle, comparison of these predictions with experiment should permit a choice among them. The energy dependence of the 180° differential charge-exchange

cross section was previously not well known. There were experimental values[1-3] for pion beam momenta up to 40 GeV/c, but they were widely spaced and generally had large statistical uncertainties. Therefore, we have measured this cross section for 52 values of pion beam momentum from 1.8 to 6.0 GeV/c using a constant-geometry experimental arrangement to eliminate sources of relative error. The average statistical uncertainty of our values is ~5%, and the possible sources of systematic error result in an estimated uncertainty of ~10% in the absolute values of the cross sections. This, however, is essentially an uncertainty in the over-all scale, not an uncertainty in the relative values of the cross sections for different momenta. In the interim since the conception of this experiment, other groups have published 180° differential cross-section values for selected pion momenta up to 18 GeV/c.[4-6]

In this paper we discuss the details of our experiment and of the analysis of the data. We present the results, previously published in brief form,[7] and a comparison of these with the results of other experiments. In addition to discussing the general features of these data, we compare them with the predictions of a dual-resonance model[8] in which the pion-nucleon amplitudes are a linear combination of Veneziano terms[9] modified by introducing a common linear imaginary part into all the Regge trajectories. We also present a compilation of 180° differential cross sections for $\pi^- p$ and $\pi^+ p$ elastic scattering and the conclusions that can be drawn from these and the charge-exchange cross sections about the isotopic-spin-$\frac{1}{2}$ and -$\frac{3}{2}$ amplitudes.

The design of a constant-geometry experimental arrangement useful for such a wide range of pion momenta was possible because the laboratory momentum of outgoing neutral pions emitted at 180° changes very little in this range [see Fig. 1(b)]. Since the minimum opening angle between the photons emitted in the decay of the π^0 is $2\cos^{-1}(p_{\pi^0}/E_{\pi^0})$, this also changes very little for the range of π^- momenta covered [Fig. 1(a)]. The detector used to detect the photons from the π^0 decay was a shower-counter hodoscope in the shape of an annular ring centered on the beam axis. The dimensions were chosen to optimize the probability that both photons from π^0's produced at 180° would impinge on the ring. Because of the slow variation of minimum opening angle, these dimensions did not change very much within the range of π^- momenta covered, and a constant geometry was found that was suitable for all momenta. The outgoing neutron was also detected by using a constant-geometry neutron detector centered on the beam axis, and data were taken with and without the requirement of neutron coincidence. An anticoincidence

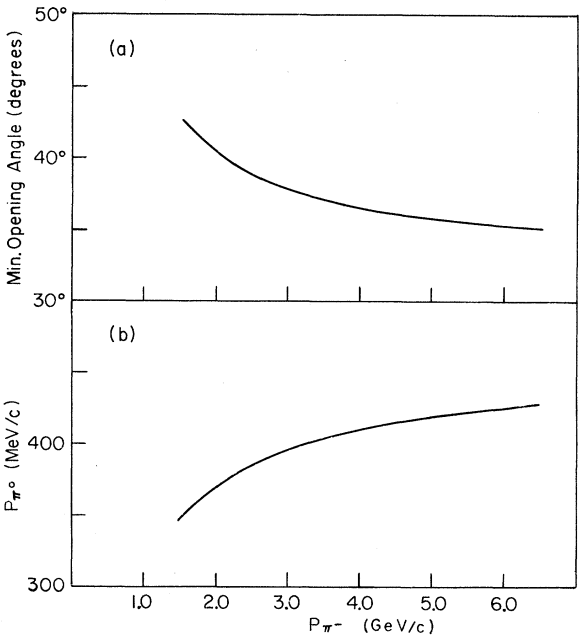

FIG. 1. (a): The minimum opening angle between the two γ rays from the decay of a π^0 produced at 180° in the reaction $\pi^- p \to \pi^0 n$. (b): The momentum of the π^0; both as functions of π^- momentum.

charge particle and shower detector surrounding the target was used to eliminate events where charged particles or multiple π^0's were produced. The individual detection efficiencies of these detectors were determined experimentally, and the over-all detection efficiency, including the details of the geometry, was calculated from a Monte Carlo simulation of the experiment.

II. EXPERIMENTAL DETAILS

A. Beam and Target

This experiment was performed in the 17° beam[10] at the Zero Gradient Synchrotron (ZGS) at Argonne National Laboratory. This facility is shown in Fig. 2. The internal beam of the ZGS was incident on the tungsten target which was also used to extract protons for the first external proton beam. During most of our experiment the target position was chosen primarily to optimize the extraction efficiency and emittance for this proton beam, and this is not generally the optimum position for yield in the 17° beam. However, the yield was 2 to 3 $\times 10^5$ pions per 10^{12} protons in the momentum region between 2.5 and 4 GeV/c. At lower and higher momenta it fell off due to the unfavorable geometry. Typically, the beam pulses were 700 m sec

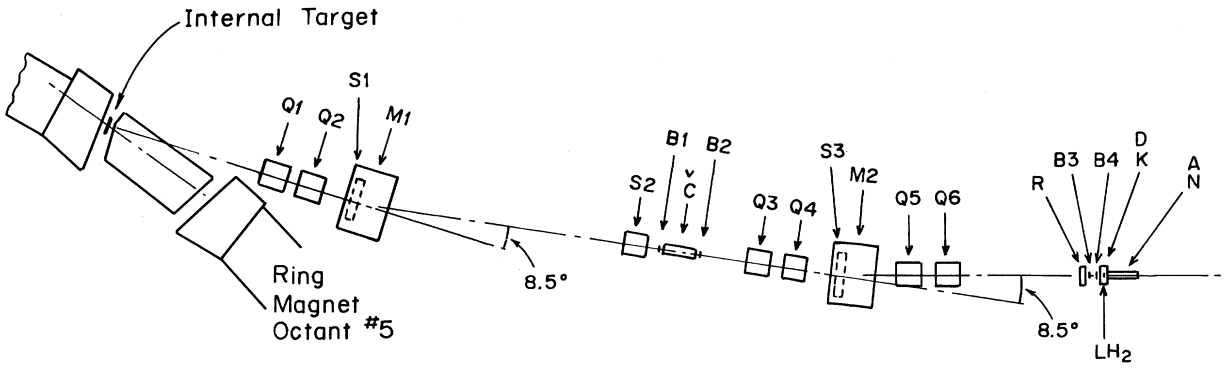

FIG. 2. The experimental layout at the ANL ZGS 17° beam. $Q1$, $Q2$, $Q3$, $Q4$, $Q5$, $Q6$, quadrupole-focusing magnets. $S1$, $S2$, $S3$, beam collimators. $M1$, $M2$, bending magnets. $B1$, $B2$, $B3$, $B4$, beam-defining scintillation counters. $\check{C}$, Čerenkov counter. R, ring (π^0) hodoscope. D, K, A, anticoincidence counters. LH_2, liquid-hydrogen target. N, neutron counter.

long and contained 2.5×10^5 π^- per pulse.

The pion beam line contains two bending magnets (M_1, M_2) and three quadrupole doublets (Q_1, Q_2, Q_3, Q_4, Q_5, Q_6).[11] Collimator S_1 defined the solid angle. Collimator S_2 at the first beam focus was set to a momentum acceptance of $\Delta p/p = \pm\frac{3}{4}\%$.

B_1, B_2, B_3, B_4, are scintillation counters and $\check{C}$ is a variable threshold Freon Čerenkov counter 9 ft long. B_1 and B_2 are disk-shaped counters, $4\frac{1}{2}$ in. diam by $\frac{1}{4}$ in. thick, positioned respectively immediately upstream and downstream from $\check{C}$. Their diameter was chosen to completely cover the two windows of $\check{C}$. B_3 and B_4 are also disk-shaped, respectively, $1\frac{1}{2}$ in. diam by $\frac{1}{16}$ in. thick and $\frac{1}{2}$ in. diam by $\frac{1}{32}$ in. thick. B_3 is placed 90 cm upstream from the center of the liquid-hydrogen (LH_2) and B_4, adjacent to the upstream window of LH_2. At beam momenta above 2.0 GeV/c, the pressure in $\check{C}$ was chosen so that π^- particles were detected but not the K^- and p^- components of the beam (~1%). Thus, the requirement for a "good" beam particle was the coincidence $B_1, B_2, B_3, B_4, \check{C}$. At beam momenta $\leq$2.0 GeV/c such a high gas pressure was required to detect π^- that the beam flux would have been reduced by interactions in $\check{C}$. Thus, since the K^- and p^- contamination were negligible, $\check{C}$ was emptied, and the requirement for a "good" beam particle was just B_1, B_2, B_3, B_4.

The liquid-hydrogen target (LH_2) was at the second focus of the π^- beam. It was a Mylar cylinder 2 in. in diameter and 21 cm long enclosed in a cryogenic jacket. The average temperature and pressure were 22.2 °K and 25.2 ± 0.5 psia, corresponding to a density of 0.0678 ± 0.0002 g/cm^3. The size of the beam spot in LH_2 was defined by B_4 and was ~$\frac{1}{2}$ in. in diameter. The angular divergence of the beam was ±5 mrad vertically.

The e^- and μ^- contamination of the beam was determined at each momentum by measuring the detection efficiency of beam particles ($B_1, B_2, B_3, B_4\check{C}$/$B_1, B_2, B_3, B_4$) as a function of Čerenkov-counter gas pressure. A typical result, the measurement for 3.0 GeV/c, is shown in Fig. 3. Figure 4 shows the values calculated from such measurements for the composition of the beam as a function of mo-

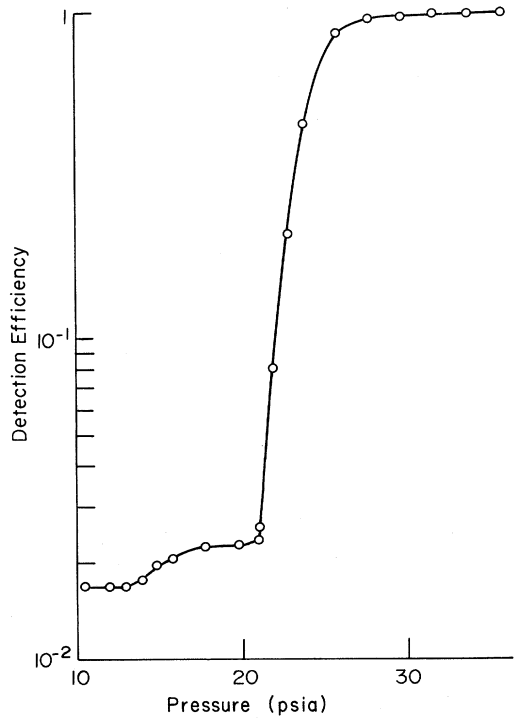

FIG. 3. The detection efficiency of the Čerenkov counter as a function of gas pressure for the 3.0-GeV/c π^- beam.

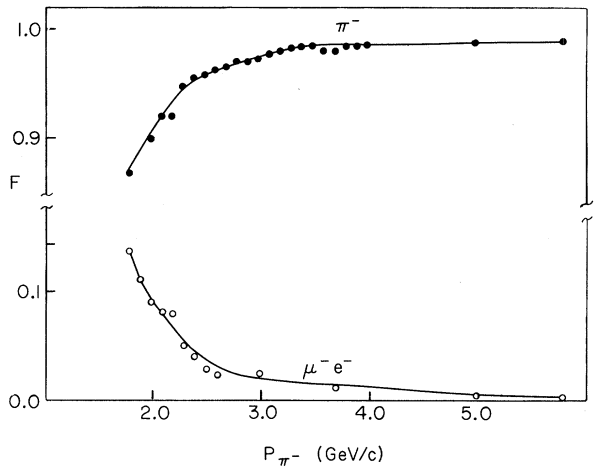

FIG. 4. Composition of the beam as a function of π^- momentum. Top curve: π^- fraction of beam. Bottom curve: $\mu^- e^-$ fraction of beam.

mentum. These values were used to correct the value for the beam flux for cross-section calculations.

B. Interaction Detection Equipment

The counters used to define a good charge exchange event are shown in Fig. 5. The liquid-hydrogen target (LH_2) is surrounded on six sides by charged particle detectors and on five sides with shower counters (P, A, K, D). One condition required for a "good" event is that no element of this charged-particle–γ-ray anticoincidence shield fires, ensuring that a beam particle has interacted, and that no charged particle and only γ rays in the backward direction were produced. γ rays from the decay of the π^0 are detected by the annular shower counter (R) upstream from LH_2. The neutron detector (N) is located downstream from LH_2.

The four lateral (D) and the downstream (K) counters of the anticoincidence shield form an enclosure of 61 by 44 cm. They contain a $\frac{1}{4}$-in. layer of scintillator followed by 9 layers of shower counter consisting of one radiation length[12] (5.8 mm) of lead, 6 mm of scintillator, and 2 mm of steel for support. Figure 6 shows the D counter arrangement and Fig. 7, the K counter. There is a 6-cm-diam hole in the K counter through which pass the beam particles which have not interacted in the target. The radiation lengths are such that the D and K counters should detect all but 0.01% of single γ rays and all but 8×10^{-5}% of π^0's (two γ rays) incident on them normally.

The A counter is designed to detect noninteracting beam particles and other charged particles and γ rays passing through the hole in the K counter without presenting a large interaction probability for forward going neutrons. It is 16 by 18 cm and consists of two layers of scintillator 6 mm thick sandwiching a single layer of lead 3 radiation lengths thick. It should detect all but 11% of single γ rays and all but 1% of forward going π^0's. 11% of forward-going neutrons interact in the A counter.

The P counter is a charged-particle detector covering the upstream hole in the anticoincidence

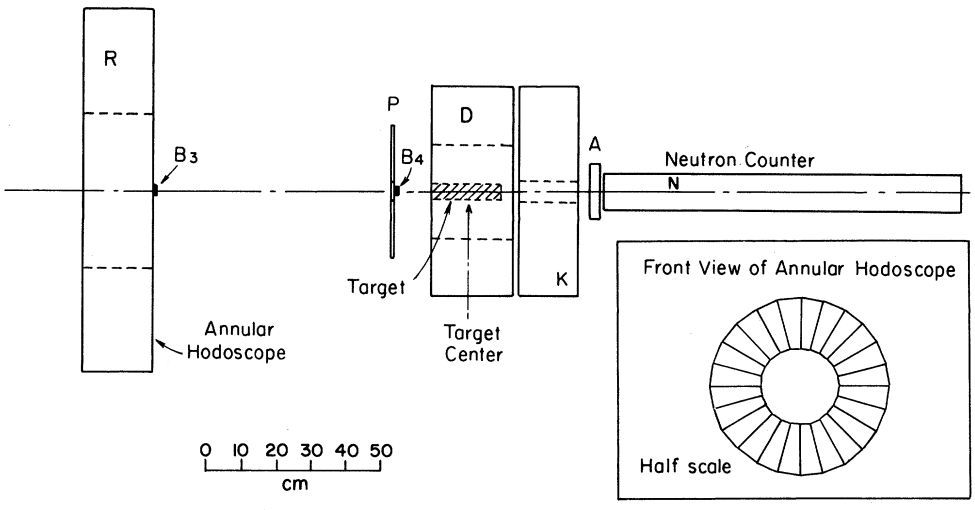

FIG. 5. Cross-sectional view of the experimental arrangement of counters. R, annular hodoscope for π^0 detection. B_3, B_4, beam-defining counters. P, backward charged-particle detector. D, K, anticoincidence charged-particle and shower detectors. A, forward anticoincidence γ detector. N, neutron counter.

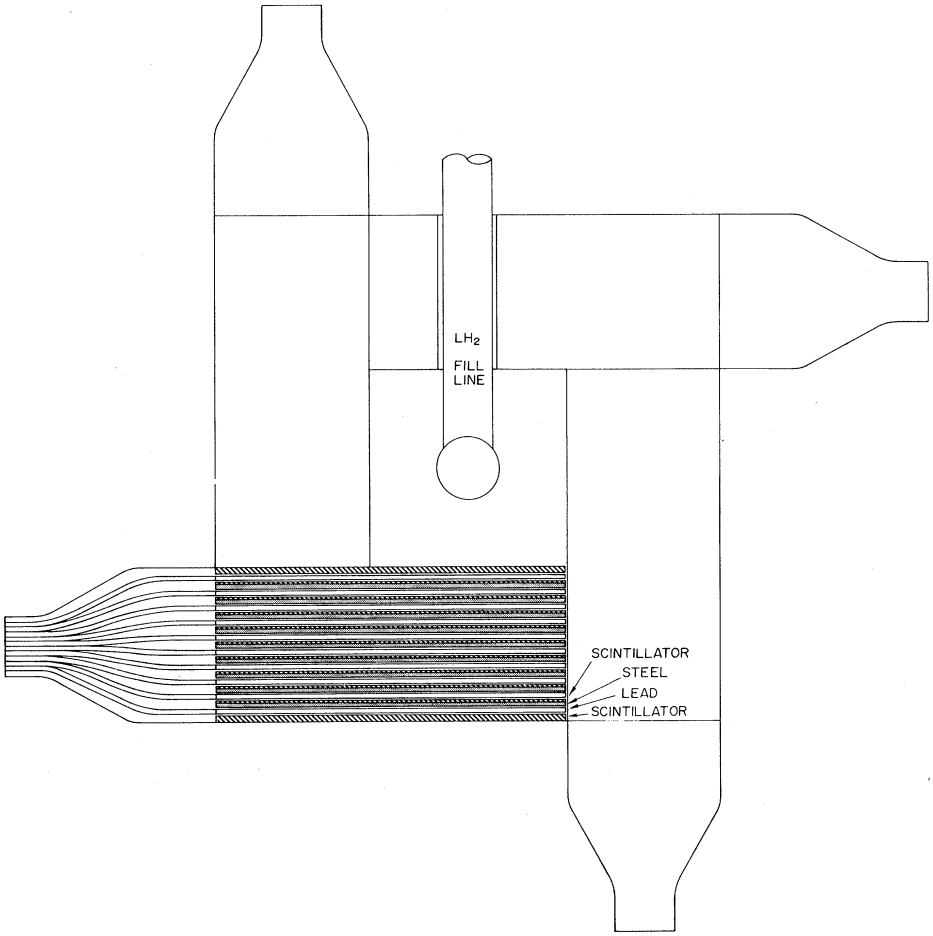

FIG. 6. Cross-sectional view of the arrangement of the D, anticoincidence detectors. The beam is coming out of the paper through the LH_2 target center. Details of the construction of one of the D counters are indicated.

shield. It consists of a piece of $\frac{1}{4}$-in.-thick scintillator, and 1.7% of backward-going γ rays are converted in it. There is a 1-in.-diam hole through the center of P for the incoming beam.

The R counter is an annular array of 24 shower counters for detecting the γ rays from the π^0 decay. It is 106 cm in outside diameter and 46 cm in inside diameter and is placed 90 cm upstream from the center of LH_2. A schematic drawing of the R counter array is shown in Fig. 5 and a more detailed drawing of one of the R shower counters in Fig. 8. These shower counters consist of eight layers, each containing 1 radiation length of lead, $\frac{1}{4}$ in. of scintillator and 2 mm of steel for support. They detect all but 0.3% of single γ rays at normal incidence. Each of the R counters contains a fitting into which pulsed light sources may be inserted to facilitate relative timing adjustments in the electronics. The photomultipliers[13] for these counters were especially selected for low noise.

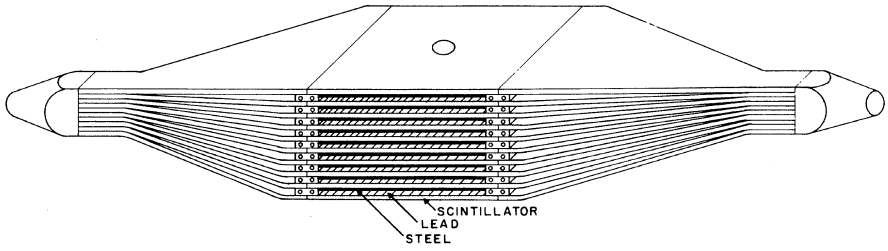

FIG. 7. The K anticoincidence detector. The central hole is for the π^- beam.

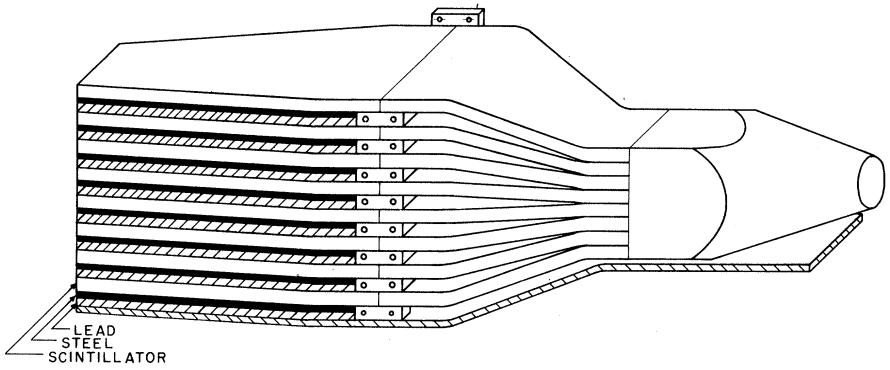

FIG. 8. One section of the R annular hodoscope.

The neutron detector N is situated with its entrance 40 cm downstream from the center of LH_2, next to the A counter. It consists of five modules 15.2 by 15.2 by 23 cm long. Figure 9 is a schematic drawing of one of these modules. It contains six layers of 2.03-cm-thick lead alternated with 1.2-in. scintillator. Thus, the N counter contains a total of 61 cm or 3.4 reaction lengths[14] of lead and ideally detects 96.7% of all neutrons traversing its whole length. The detection efficiency for this counter as used in this experiment was determined experimentally and is in agreement with the theoretical figure. This will be discussed in Sec. II D.

C. Electronic Logic and Data Storage

The basic definition of a good event was one for which there was a good beam particle ($B_1, B_2, B_3, B_4, \check{C}$), for which no counter in the anticoincidence shield fired ($\overline{AD_1D_2D_2D_4KP_1P_2}$) and for which two or more ring counters fired ($R_iR_j \ldots, i \neq j$). In addition, it was necessary to determine whether there was a neutron in coincidence (N) and to record the rate of accidental coincidences. The logic used to achieve this is shown in Fig. 10. A beam trigger ($B_1B_2B_3B_4\check{C}\overline{P_1P_2}$), a ring counter trigger ($R_iR_j \ldots, i \neq j$) and an anticoincidence shield trigger ($\overline{AD_1D_2D_3D_4K}$) were formed. If there was a coincidence between them, a master trigger was formed. To measure the rate of accidentals the beam trigger was delayed by 70 nsec, the period of the rf structure. If there was an accidental coincidence between this delayed trigger, a ring counter trigger and an anticoincidence shield trigger, a master trigger was formed but was accompanied by an accidental marker pulse. If there was a neutron counter pulse in coincidence with the master trigger, a neutron marker pulse was generated. The beam trigger pulses were counted to provide information on the incoming flux for the cross sections. Various other pulses were counted

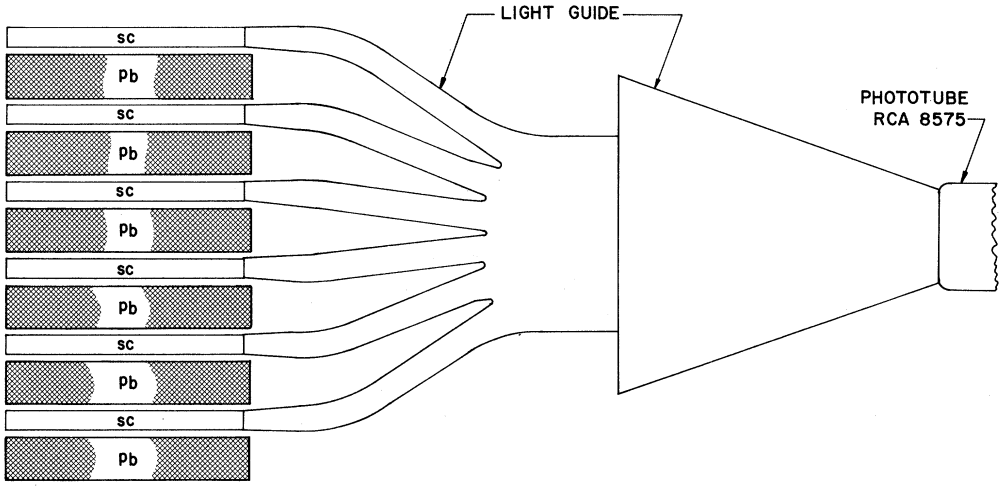

FIG. 9. One of the N neutron counter modules.

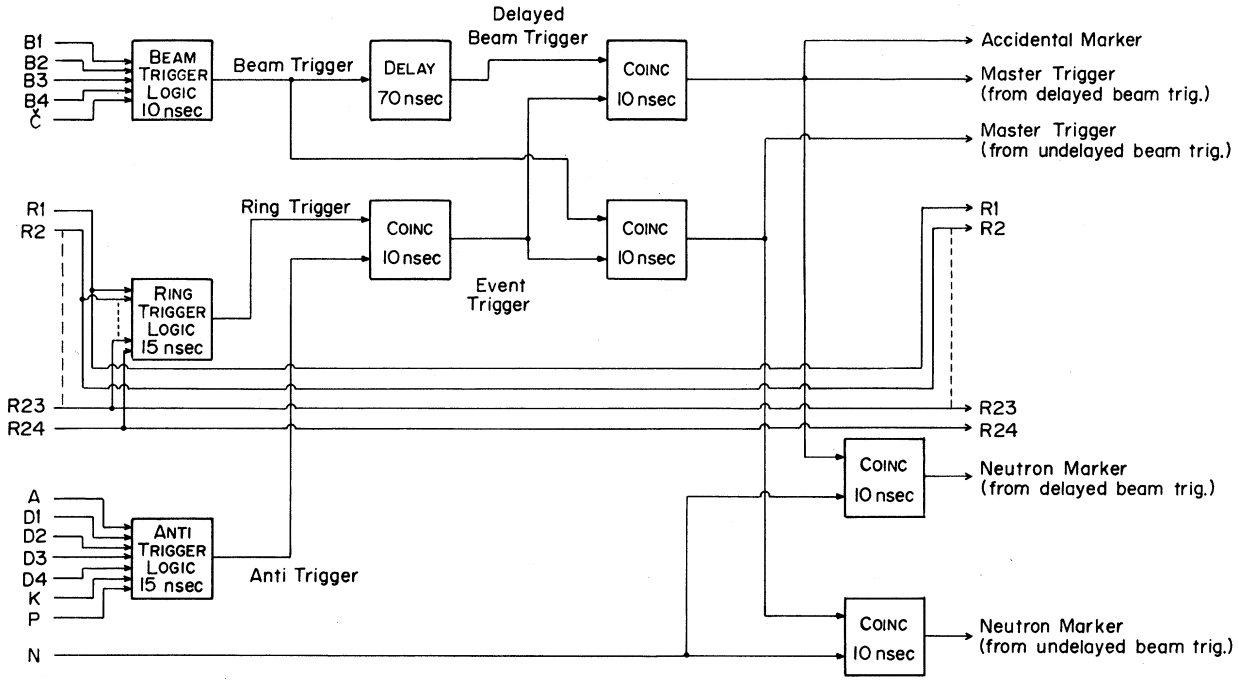

FIG. 10. Schematic diagram of the logic used to define the backward π^0 events.

to provide checks on equipment performance.

Figure 11 shows the master-trigger counting rate (*RB*) and the neutron marker pulse counting rate (*RBN*) as a function of the delay between the beam trigger and the ring counter trigger. The width of both peaks is ~23 nsec which arises from the 8-nsec width of the beam trigger and the 15-nsec width of the ring counter trigger. The accidentals rate is seen to be ~10% for *RB* and ~5% for *RBN* pulses.

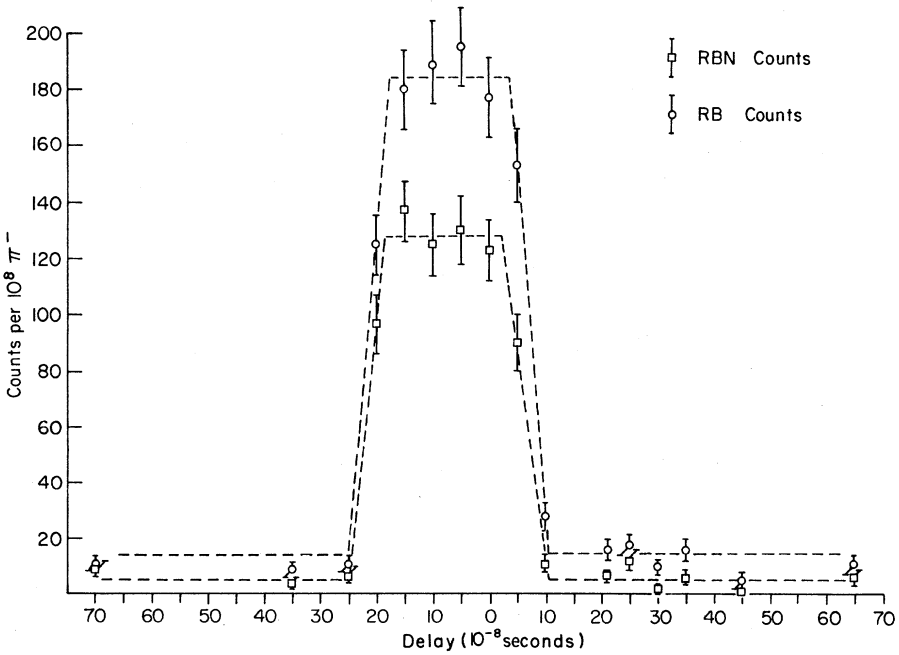

FIG. 11. The master-trigger counting rate with neutron coincidence required (*RBN*) and without neutron coindidence required (*RB*) as a function of the delay between the beam trigger and the ring counter trigger.

The information to be stored for each event was the following: Which of the 24 ring counters fired, whether there was a neutron marker, and whether there was an accidental marker, a total of 26 bits. The signals from the ring counters were suitably delayed (~120 nsec) to arrive at the input gate to the storage buffer in coincidence with the master trigger, the neutron marker, and the accidental marker. If there was a master trigger, the gate was enabled, and the 26 bits were passed into the main storage buffer. In addition to the main storage buffer, there were ten further storage buffers, each capable of storing 26 bits, to which the information was transferred. While the information was being stored in the main buffer and was being transferred out of the main buffer, the counter logic system was not enabled. When the main buffer was emptied, a ready flag was sent to enable the counter logic. This system could therefore accept up to 11 events per machine pulse at a rate of 125 kc.

The information in the storage buffers was read out into two systems. One was a hardware logic interface (Marbles) feeding into registers and a Flexowriter with printout and a punched paper tape unit. The second, which was only available for the latter half of the experiment, was a PDP-8/S with a teletype and a punched paper tape unit. For both systems, the 26 bits of storage buffer were scanned by a commutator at a rate of 250 kc. When a bit was encountered, the scanning stopped; the bit number was stored by Marbles and read out to the Flexowriter and the PDP-8/S. When this was completed, the scanning was resumed until the next bit was encountered.

The output information from Marbles was recorded by 24 "counter" registers, one corresponding to each ring counter, and by 11 "difference counter" registers. When a bit number was detected by Marbles, the corresponding counter register was incremented by one, providing no accidental marker had been read. The distribution in the counters was an immediate check on their performance. The Flexowriter recorded the bit number on the printout and punched paper tape for the counter, accidental marker, and neutron marker bits. When the first bit was encountered by the scanner, a modulo 12 up-down counter was started which was stopped when the second bit was encountered. After the 24 counter bits were scanned, the content of the up-down counter, which represented the difference counter number, was then stored by incrementing by one the corresponding difference counter register providing no accidental marker had been read.

The PDP-8/S output on printout and paper tape was identical with that of the Flexowriter. In addition, it formed internal histograms in real time which were printed out and punched on paper tape at the end of each run. These included various counter distributions and also difference counter distributions, both with and without neutron and accidental markers.

The difference counter number was defined as follows. If only one of the 24 counter bits or only two adjacent counter bits were on, this was a one-γ-ray event, and a difference counter number was not generated. If the bits in nonadjacent counters were on, then the number in the up-down scaler, which is the smallest number of intervening counters plus one, was taken as the difference counter number (e.g., if counters 1 and 9 fire, the difference counter number was 8. If counters 1 and 17 fire, the difference counter number was also 8). If one isolated counter and a pair of adjacent counters register events, then this was taken as a two-γ-ray event because a shower originating in the edge of one counter could also trigger an adjacent counter. The difference counter number was taken to be that associated with the largest physical separation (e.g., if counters 1, 9, and 10 fired, the difference counter number was 9). Similarly, if two pairs of adjacent counters fired, this was taken as a two-γ-ray event, and the difference counter number was taken to be that associated with the largest physical separation. This choice did not introduce any biases since the same choices were made in the Monte Carlo programs used to generate difference counter distributions for geometric detection efficiency factors. Counter difference numbers were not generated for cases with three or more separate hits.

D. Shower-Counter and Neutron-Counter Detection Efficiencies

The physical detection efficiency of a ring shower counter was measured at the University of Illinois betatron and found to be better than 99% for 100- and 200-MeV/c electrons and positrons. This agrees with the ideal result that only 0.3% of all γ rays at normal incidence will not convert in 8 radiation lengths of matter. The complete detection efficiency including the geometric configuration was determined by Monte Carlo simulations which are discussed in Sec. III B.

The interaction cross section for neutrons in lead gives the result that 97% of the neutrons will interact in traversing the full length of the neutron counter. However, there is not a 100% probability that each interaction will result in particles that produce pulses in the scintillation counters. For example, if the neutron counter consisted of 3.4 interaction lengths of lead followed by a single

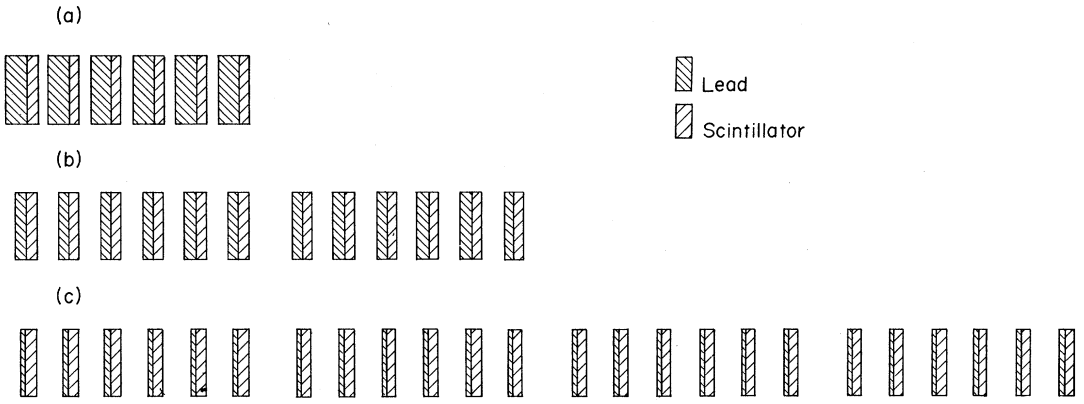

FIG. 12. The three arrangements of lead and scintillator used in the determination of the neutron counter efficiency. (a) $n=1$, (b) $n=2$, (c) $n=4$.

piece of scintillator, the particles produced by a neutron interacting in the first 0.1 interaction length would probably not reach the scintillator. If the neutron interacted close to the edge of the lead, then the probability would be reduced even further since, on the average, half of the secondary particles would leave the detector. The efficiency for detecting neutrons by a counter which consists of k pieces of lead of thickness t each followed by a slab of scintillator can be written

$$E=(1-e^{-kt/\lambda})P_D(t,1)G\,, \tag{1}$$

where λ is the interaction length, $P_D(t,1)$ is the probability that a neutron interacting in a single piece of lead of thickness t will produce a signal in the scintillator, and G is a solid-angle factor. G was calculated by our Monte Carlo simulation of the experiment, but $P_D(t,1)$ was necessarily determined experimentally.

The experiment was based on the obvious fact that all interactions will be observed if the slabs of lead are made very thin. The approach taken was to divide each thickness t into n slabs, each followed by a scintillator. Then, the probability that an interaction neutron will produce a signal becomes

$$P_D(t,n)\xrightarrow[n\to\infty]{}1\,. \tag{2}$$

Figure 12 illustrates the experimental configurations used to determine $P_D(t,n)$. In configuration (a), used in our neutron detector, $t=2.03$ cm and $n=1$. Six of such lead scintillator sandwiches are used to increase the data collection efficiency. In configuration (b), $t=2.03$ cm and $n=2$. There are twelve sandwiches each containing 1.015 cm of lead. In configuration (c), $t=2.03$, $n=4$, and there are 24 sandwiches.

Those backward charge-exchange events for which there is an RB coincidence signal involve a neutron traveling inside a narrow forward cone defined by the geometry of the π^0 detector and the kinematics. If N_{RB} is the number of such events, then the number of coincident neutron detector triggers should be

$$N_n=N_{RB}E_n\,, \tag{3}$$

where, in principle, the neutron detection efficiency is

$$E_n=(1-e^{-kt/\lambda})P_D(t,n)G_n\,. \tag{4}$$

G_n is now the solid angle factor for the particular configuration. In practice, one must also include the effects of the scintillator on the efficiency and the actual calculation was in fact carried out including these effects. However, this calculation may be represented by the following simplification. The ratio

$$R_n=\frac{P_D(t,1)}{P_D(t,n)}=\frac{E_1G_n}{E_nG_1} \tag{5}$$

may be calculated from Eq. (3), the experimental values for N_1, N_n, N_{RB}, and the values calculated for G_n and G_1 by the Monte Carlo simulation. However, from Eq. (2) we see that

$$R_n=\frac{P_D(t,1)}{P_D(t,n)}\xrightarrow[n\to\infty]{}P_D(t,1)\,. \tag{6}$$

Thus the values found for R_n should give $P_D(t,1)$ when extrapolated to sufficiently large n. Con-

TABLE I. Relative efficiency for detecting a neutron interaction in a lead scintillator array.

Beam momentum	$R_2=\frac{P_D(t,1)}{P_D(t,2)}$	$R_4=\frac{P_D(t,1)}{P_D(t,4)}$
2.2 GeV/c	1.01 ± 0.03	0.97 ± 0.03
3.0 GeV/c	0.98 ± 0.03	0.99 ± 0.03

versely, if R_n is constant, it implies that

$$P_D(t,1) = R_n . \quad (7)$$

We determined R_2 and R_4 at two beam momenta, 2.2 and 3.0 GeV/c. Table I gives the results calculated using the complete analysis including the effects of the scintillator[15] rather than the approximate method discussed above. Since the total inelastic cross section for lead is constant from 1 to 6 GeV/c,[14] we expect no efficiency variation with momentum due to the basic cross section. $P_D(t,1)$, however, could be momentum-dependent and would be expected to approach unity more closely at higher momenta. However, within the uncertainties these results are consistent with $P_D(t,1) = 1$ for both beam momenta studied. In addition to the statistical uncertainties given in Table I, there is a 4% systematic uncertainty in the interaction length in scintillator. Therefore, for the neutron counter array used in our experiment, we conclude that our efficiency for detecting a neutron interaction is unity to within 5%.

The neutron beam defined by the *RB* trigger could, of course, be used to determine the detection efficiency of other neutron counter configurations. We carried out such an investigation for a configuration very similar to that in another experiment[6] measuring the backward charge-exchange cross section. This investigation was prompted by the disagreement between the values given for neutron counter efficiencies in that experiment and what would be expected from the considerations just discussed. The configuration investigated consisted of six $\frac{3}{8}$-in.-thick by 7.2 by 9.4 in. pieces of brass spaced 1.4 in. apart and placed so that the neutron beam defined by the *RB* trigger was centered 2 in. from one edge of this array. We placed a scintillation counter behind the brass array so as to just cover the brass. We placed a second counter with ten times the area of the brass array behind the first scintillation counter. Hence, we could measure how many neutrons produced interactions such that the charged fragments went sufficiently forward so as to pass through all the brass, and also how many passed out of the edge of the array without getting to the smaller counter. Both counters were placed in coincidence with our *RB* logic. Our measurement showed that for 40% of the interactions occurring within 2 in. of the edge of the brass array, the resultant charged particles left the edge of the array before getting to the small counter and were recorded in the larger counter. This measurement was performed at an incident beam momentum of 3 GeV/c. The effect would be greater at lower momenta and is not consistent with the neutron counter efficiencies quoted in Chase *et al.*[6]

III. DATA ANALYSIS

A. Corrections

The raw data used to calculate the cross sections consisted of the difference counter distributions with (*RBN*) and without (*RB*) neutron coincidence required. In addition to real two-γ-ray events from π^0's originating in the hydrogen, these include events from coincident γ rays originating elsewhere and accidental coincidences. A possible source of background would be γ rays from multiple π^0's produced in the hydrogen. However, an investigation of this possibility showed that the contribution to the counting rate was negligible. This is discussed in Sec. III D.

All of the background from nonhydrogen events was removed by subtracting the difference counter distribution obtained with LH_2 empty from that obtained with LH_2 filled with liquid hydrogen at each momentum. Figure 13 shows the counting rates for the sum of the *RBN* events in the difference counter distributions for target full and target empty as a function of incoming π^- momentum. The subtraction is seen to be $\lesssim 5\%$ over the whole range. For *RB* events the subtraction was $\lesssim 10\%$ over the whole range.

The singles counting rates for the ring counter trigger with target full and target empty were equal to within 1% and, therefore, most of the accidental events were also removed by the subtraction of the empty target events. There is one class of accidental events for which this is not true. This is the case where a π^0 from the hydrogen decays so that only one γ ray is incident on the ring counter and is in accidental coincidence with a non-hydrogen event in the ring counter. The contribution of this type of accidental to the difference counter distribution should be constant with respect to difference counter number (i.e., if a γ ray from a hydrogen fires a given counter, an accidental coincidence with any other counter is equally probable). Since the difference counter distribution from π^0 events is peaked (see Sec. III B), these accidentals are observed as a filling in of the difference counter number region not populated by π^0 events. A correction for this effect was calculated from the singles rates in the ring counters. Figure 14 shows the raw difference counter data for 3 GeV/c, the target-empty subtraction, the accidental subtraction, and the corrected data. The solid line is the Monte Carlo prediction (see Sec. III B) for the π^0 difference counter distribution. The corrected data are observed not to populate the region of the difference counter distribution predicted to be empty by the Monte Carlo calculation, indicating that the background and accidental subtraction did include all contribution sources.

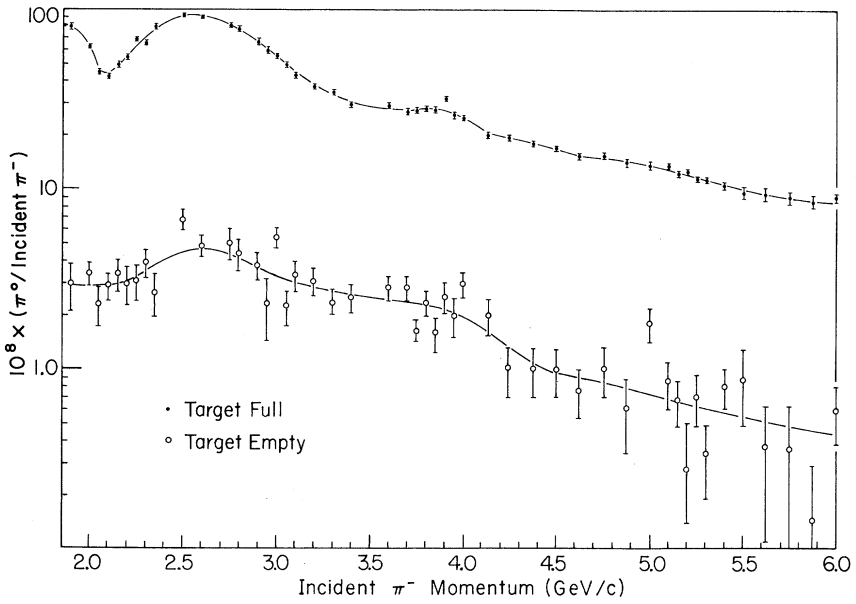

FIG. 13. Comparison of the counting rates for target empty and target full as a function of π^- momentum.

B. Monte Carlo Simulation

A Monte Carlo program simulating the experimental situation was used in optimizing the design of the equipment and to calculate the detection efficiency for π^0's. Charge-exchange events for given π^- momentum and π^0 angular distributions were thrown with a vertex position chosen randomly in a volume corresponding to the beam dimensions in the target. The beam direction for each event was chosen randomly inside the beam cone. The neutron and both γ rays from the decay of the π^0 were allowed the probability of interaction with any matter encountered along their paths according to their elastic and inelastic cross sections and conversion probabilities for that matter (iron, lead, or scintillator).[13,15,16] If an interaction took place in a counter, a trigger was registered for that counter. If the neutron scattered elastically in the A counter, it was terminated at that point but an A counter trigger was not registered. If a γ ray interacted in a ring counter within 1 cm of the edge of an adjacent counter, triggers were registered for both counters. Similarly, if a γ ray interacted in a crack, triggers were registered for both counters. Difference counter numbers were calculated for all events where both γ rays triggered at least one ring counter using the same rules as those applied in the Marbles logic (see Sec. II C).

The initial problem was to choose the optimum ring counter geometry for π^0 detection for the whole range of momenta. Figure 15 shows a cross sectional view of the ring counter, the opening angle distribution for an ~400-MeV/c π^0 produced at 180° by a 3-GeV/c π^- and the energy of the γ rays as a function of their angle with respect to the π^0 direction. One would expect that the optimum geometry would be one where the sum of $\theta_{\min}$ and $\theta_{\max}$ as defined in Fig. 13 would be equal to the

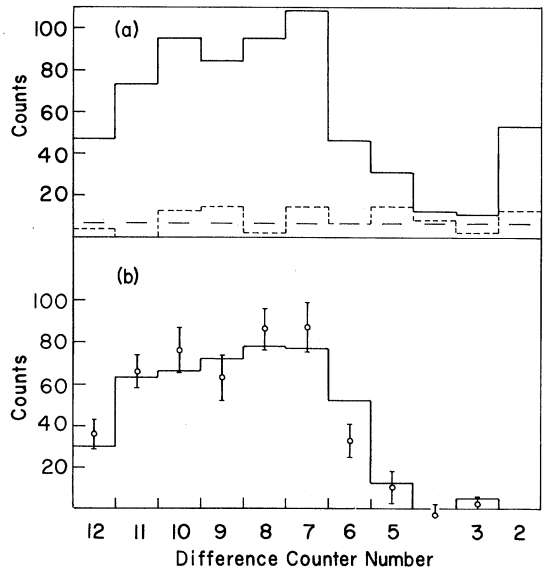

FIG. 14. Difference counter distributions for π^0's produced by 3-GeV/c π^- particles. (a) Solid histogram: raw data, target full; dashed histogram: raw data target empty (normalized to the same number of incident particles); broken line: counts due to accidental coincidences. (b) Points: data after subtraction of target-empty and accidental backgrounds; histogram: Monte Carlo prediction.

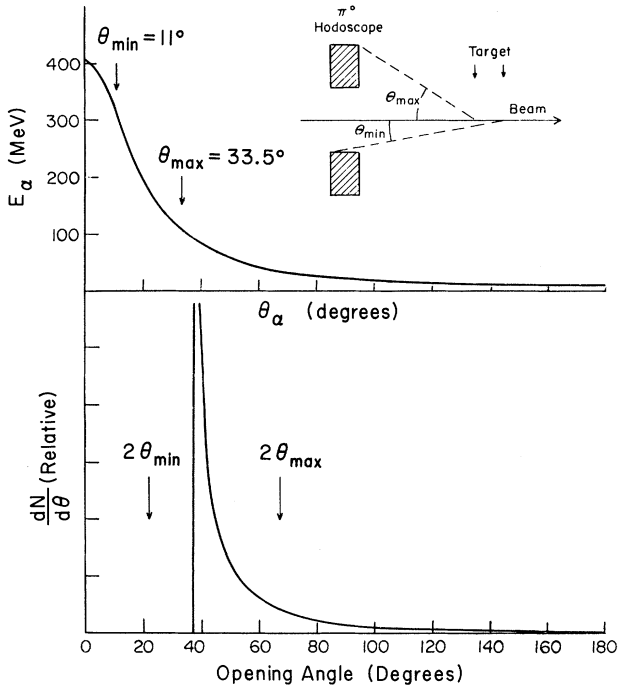

FIG. 15. Top curve: the energy of the γ rays from the decay of a π^0 produced at 180° by a 3-GeV/c π^- particle as a function of the decay angle of the γ ray. The insert is a cross-sectional view of the geometry defined by the target and the π^0 hodoscope. Bottom curve: the probability that the π^0 will decay with a given opening angle between the γ rays as a function of opening angle.

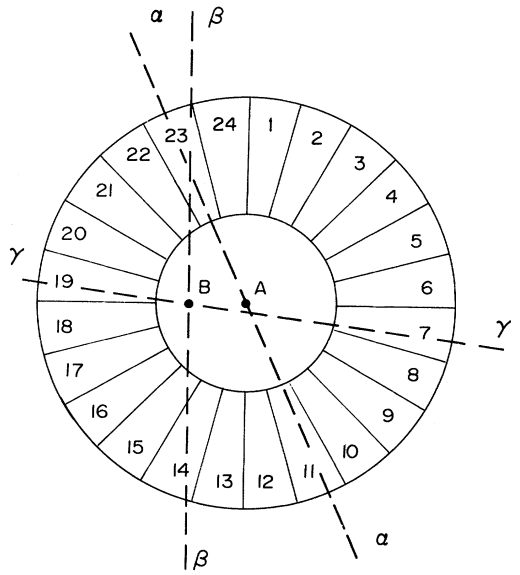

FIG. 16. Schematic view of the front face of the π^0 hodoscope. If a π^0 is produced at 180°, the γ rays from its decay will intersect a line passing through the center (A) of the ring (for example, line α). Thus the γ rays will always trigger opposite counters. If a π^0 is produced at 170°, its line of motion will intersect the front surface of the hodoscope of B and the decay gamma rays will intersect lines such as β and γ and all intermediate possibilities. Thus, other pairs of counters in addition to those directly opposite will be triggered. At the exit face point B is shifted further from the center; A, obviously, remains centered.

minimum opening angle. θ_{min} and θ_{max} were chosen to optimize the π^0 detection efficiency at 180° without increasing the range of angles for which the π^0 could be detected. The results depended on the beam momentum but not very strongly as expected from the slow change in the minimum opening angle with π^- momentum (see Fig. 1). Since the lowest counting rates were expected at 6 GeV/c, the optimum conditions for 6 GeV/c were chosen: $\theta_{min} = 11°$ and $\theta_{max} = 33.5°$. From the opening angle distribution in Fig. 15 it is seen that this choice brackets the minimum opening angle for 3 GeV/c as would be expected. The energies for γ rays with angles below θ_{max} are above 100 MeV where our shower counter efficiency measurements apply.

γ rays from the decay of π^0's produced at 180° with respect to the beam axis will always trigger opposite counters in the ring counter. This is illustrated in Fig. 16. Such events will always have a difference counter number of 12 if only two counters are triggered. However, a π^0 traveling at 170° with respect to the beam axis could result in any difference counter number between 3 and 12 inclusive. The range in production angle for which π^0's will be detected by the ring counter is shown in Fig. 17 for 2-, 4-, and 6-GeV/c beam momentum. These curves give the percentage of π^0's produced in a given cosine interval $P(\cos\theta)$ that would be detected by the complete system (RBN events) as a function of the cosine of the π^0 angle (θ). The weighted average value of the cosine of the π^0 angle,

$$\cos\theta_{av} = \frac{\sum P(\cos\theta)\cos\theta}{\sum P(\cos\theta)} ,$$

is indicated on each histogram. This was considered to define the effective π^0 angle for each momentum. The interval between $\cos\theta = -1$ and $\cos\theta = 2(\cos\theta_{av}) + 1$ contained ~95% of the events at all momenta.

C. Cross-Section Calculations

The number of counts in the ith difference counter bin is

$$N_i = 4\pi N_{\pi^-} N_{LH_2} \int_{-1}^{1} \frac{d\sigma}{d\Omega}(\cos\theta) P_i(\cos\theta) d(\cos\theta) , \qquad (8)$$

where N_{π^-} is the beam flux, N_{LH_2} is the number of target atoms per cm^2, $(d\sigma/d\Omega)(\cos\theta)$ is the differential cross section as a function of the cosine of

the π^0 angle θ, and $P_i(\cos\theta)$ is the probability that a π^0 produced between $\cos\theta$ and $(\cos\theta+\Delta\cos\theta)$ will trigger the ring counter so that the difference counter number is i. The integral can be replaced by a sum

$$N_i = 4\pi N_{\pi^-} - N_{\mathrm{LH}_2} \sum_j \frac{d\sigma}{d\Omega}(\cos\theta_j) P_i(\cos\theta_j)\Delta\cos\theta\,, \qquad (9)$$

where $\Delta\cos\theta$ is small. Since $P_i(\cos\theta_j)$ is zero for all angles not close to 180°, only terms for which $(-1-\cos\theta_j)$ is small are nonzero. Thus $(d\sigma/d\Omega)\times(\cos\theta_j)$ is replaced by $(d\sigma/d\Omega)(-1-\cos\theta_j)$ and expanded about 180° as follows:

$$\frac{d\sigma}{d\Omega}(-1-\cos\theta_j) = \left(\frac{d\sigma}{d\Omega}\right)_{180^\circ} + \left[\frac{d}{d\cos\theta}\left(\frac{d\sigma}{d\Omega}\right)\right]_{180^\circ} \times(-1-\cos\theta_j)\,. \qquad (10)$$

Therefore

$$N_i = 4\pi N_{\pi^-} - N_{\mathrm{LH}_2}\left\{\left(\frac{d\sigma}{d\Omega}\right)_{180^\circ}\Delta\cos\theta\sum P_i(\cos\theta_j) + \left[\frac{d}{d\cos\theta}\left(\frac{d\sigma}{d\Omega}\right)\right]_{180^\circ}\Delta\cos\theta\sum P_i(\cos\theta_j)(-1-\cos\theta_j)\right\}. \qquad (11)$$

The $P_i(\cos\theta_j)$'s are obtained from the Monte Carlo simulation and, therefore, the N_i's, the difference counter distributions, can in principle be fitted by this expression obtaining values for the differential cross section $(d\sigma/d\Omega)_{180^\circ}$, and the slope of the differential cross section, $[(d/d\cos\theta)(d\sigma/d\Omega)]_{180^\circ}$. The beam flux N_{π^-} was corrected for contamination by μ mesons and electrons, and the N_i were corrected for background and accidentals as previously discussed (Secs. II A and III A, respectively).

The dependence of the difference counter distribution on the angular distribution of the π^0 is not strong, because the angular interval accepted is so small. Figure 18 shows the Monte Carlo difference counter distributions for 6-GeV/c π^- momentum for several slopes including −10% which is approximately the value indicated by the data of Schneider *et al.*[4] and Boright *et al.*[5] The difference counter data of this experiment are also shown.

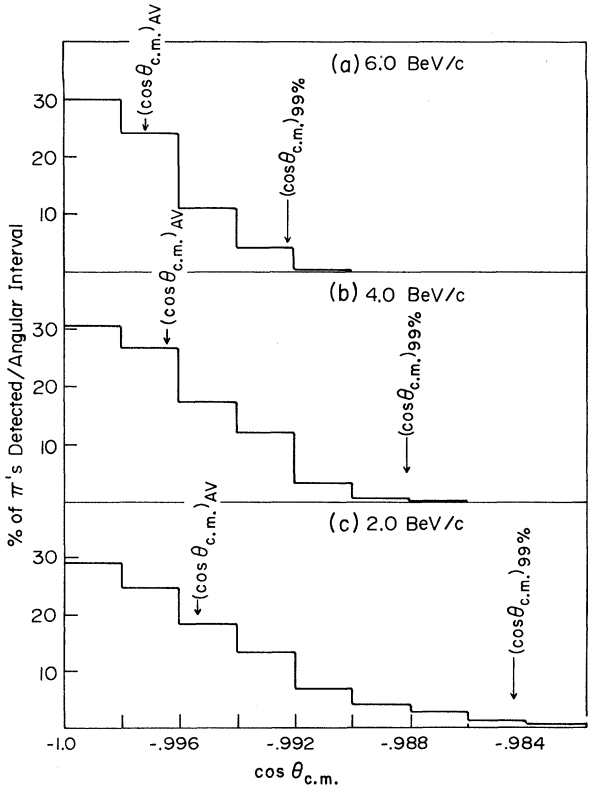

FIG. 17. The percentage of π^0's produced in a given interval in $\cos\theta_{\mathrm{c.m.}}$ which are detected by the π^0 hodoscope as a function of $\cos\theta$ for three π^- momenta.

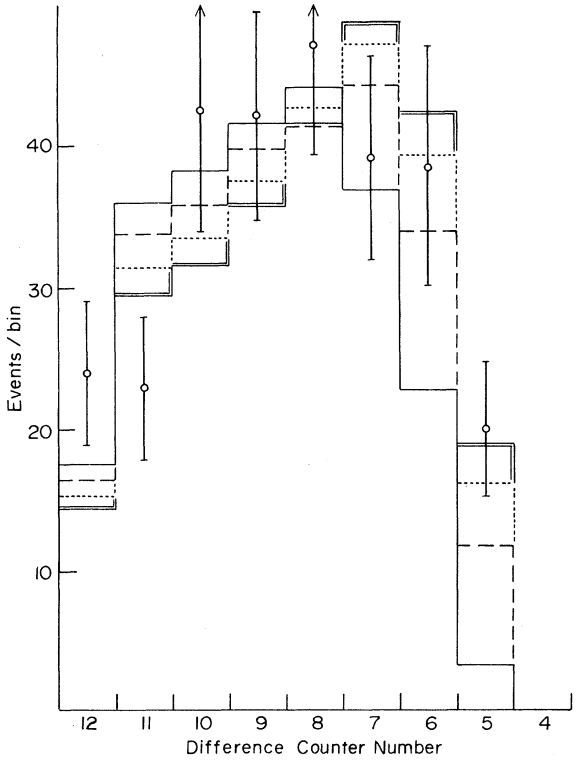

FIG. 18. Difference counter distributions for π^0's produced by 6-GeV/c π^- particles. The points are the experimental values. The solid histogram assumes an increase in $(d\sigma/d\Omega)_{\mathrm{c.m.}}$ of +30% for $\Delta\cos\theta = 0.002$. The broken histogram, +10%. The dashed histogram, − 10%. The double-line histogram, −30%.

Even for very different values of the slope, the Monte Carlo difference counter distributions are in agreement with the data. The fit of the Monte Carlo distribution for the +10% slope to the data gives the minimum value ($\chi^2 = 9$). However, the χ^2 minimum is broad, and the fit for −10% ($\chi^2 = 11$ for 7 degrees of freedom) yields an acceptable 15% confidence level. Fits to the difference counter distributions were made using both the extrapolated cross section and the slope as parameters. Above 2.7 GeV/c the uncertainties of the slopes resulting from these fits were so large that the central values were consistent with zero. At 2.7 GeV/c and below the results indicated a dependence on slope. This is understandable since, at lower momenta, the geometry permits detection of π^0's at several degrees with respect to 180°. Correspondingly, the bins corresponding to large difference counter number are very sensitive to the slope. These bins are also sensitive to the details of the counter geometry and the assumptions concerning edge effects. Therefore, the effect of successively eliminating the data in the bins with highest difference counter number from the cross section calculation was studied. This led to the conclusion that, below 2.7 GeV/c, the possible systematic uncertainty due to the slope was $\lesssim 10\%$. Above 2.7 GeV/c, this uncertainty is negligible.

The results for both the data with neutron coincidence required and that where neutron coincidence was not required are shown in Fig. 19 with typical uncertainties indicated at a few points. All the uncertainties given on differential cross sections from our data include the statistical uncertainties of the N_i, including those from subtraction of background and accidentals, and the systematic uncertainties in N_{π^-} and N_{LH_2}. The agreement between the two sets of data is excellent, yielding a χ^2 of 33 for 52 points. Since the two sets of data involved different background and accidental subtractions and different Monte Carlo probabilities this is a strong verification that the relative uncertainties given are reliable. There remains the possibility of a systematic error affecting the data with neutron coincidence identically as it affects that without. A possible source of such an effect would be incorrect hypotheses concerning the detection probability of γ rays incident on edges of the ring counters. This was checked by comparing the observed number of 2γ events firing 2, 3, and 4 counters with the Monte Carlo predictions, and the agreement was good and no correction was in-

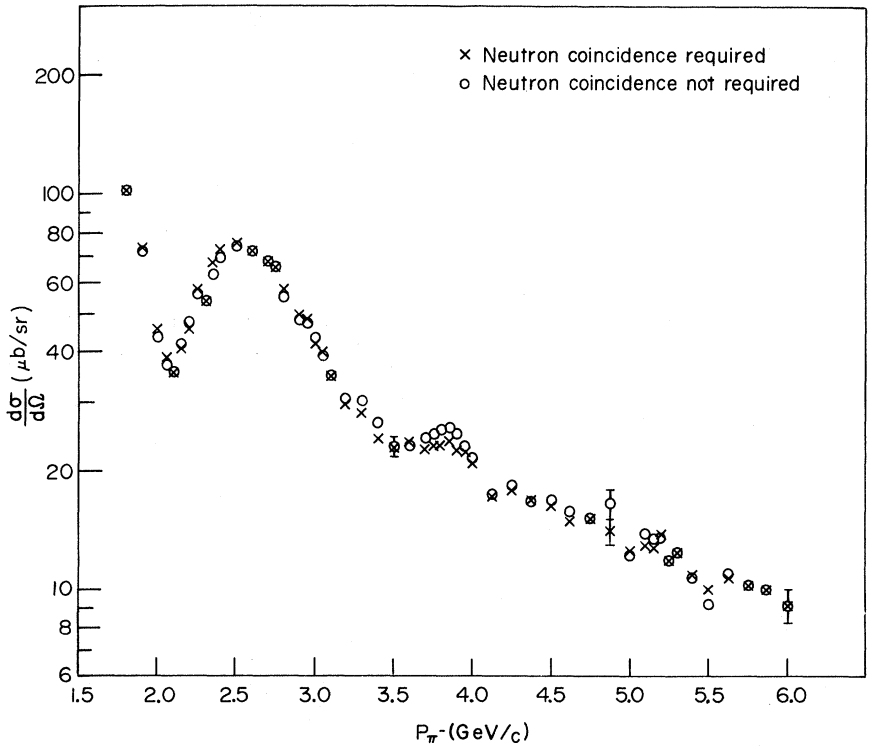

FIG. 19. Comparison of the center-of-mass differential cross sections at 180° calculated from the data where neutron coincidence was required with the center-of-mass differential cross sections at 180° from data where neutron coincidence was not required.

dicated. Another possible source of systematic error would be misalignment of the counter. The effects of various displacements of the counters on the π^0 detection probability were studied with the Monte Carlo simulations and were found to be of the order of only ~2% for sizeable (1-cm) misalignments. Therefore, the over-all systematic uncertainty in our cross sections is estimated to be $\lesssim$10% above 2.7 GeV/c and $\lesssim$14% below 2.7 GeV/c.

D. Background from Other Reaction Channels

Other reaction channels from hydrogen interactions leading to all neutral final states with at least two γ rays could in principle contribute a background not removed by empty-target subtraction. The first possibility to be considered is the production of a neutron and a heavier neutral meson, such as the η, which decays to two γ rays. However, the largest opening angle detectable by our hodoscope is 67° (see Sec. III B), which corresponds to $\gamma = E/m = 1/\sin(\frac{1}{2}\theta_{\text{opening}}) = 1.803$ for a particle decaying into two γ rays at the minimum opening angle. If this particle is produced at 180° by a 3-GeV/c pion, then the largest mass it can have is 0.246 GeV, and η's are not detectable.

The second possibility is that two γ rays from the decay of π^0's from

$$\pi^- + p \to n + K\pi^0, \quad K = 2, 3, 4, \ldots$$

trigger the ring counter and that the other γ rays do not trigger the anticoincidence shield. This latter condition is only met if all the γ rays either go backward missing the D counter or forward through the hole in the K counter and do not trigger the A counter. Practically, we need only consider the two-π^0 case, since the probability for meeting these conditions is negligible if more than two π^0's are produced. For the two π^0 case a spurious event is possible if both π^0's go backward or if one goes forward and one backward.

The contribution from the case where both π^0's go backward is expected to be small since there is experimental evidence[17] that <0.04% of the $2\pi^0$ cross section at 2.6 GeV/c would correspond to events with both π^0's produced so that their γ's could miss the anticoincidence shield. 0.8% of charge exchange events have π^0's in the appropriate cone at 2.6 GeV/c and, thus, there is a factor of 20 between the probabilities for real π^0 and fake π^0 from $2\pi^0$. The factor is actually bigger because the γ rays from a real π^0 are at the appropriate angle for detection by the ring counter, whereas the γ rays from $2\pi^0$'s are not. Monte Carlo studies of this problem indicate that the additional factor is strongly model-dependent but that a value of 10 is reasonable. Thus, since the $2\pi^0$ cross section is twice as big[2] as the π^0 cross section, one would expect less than 1% of the π^0 events to be fake π^0 from $2\pi^0$. Furthermore, the difference counter distribution would be isotropic and distinguishable. We have direct experimental substantiation that the effect is small. If $2\pi^0$ events are important, then we would expect 3- and 4-γ-ray events in the ring counter. We checked at several energies and, within the statistics, there were no multiple-γ-ray events in the data after empty-target subtraction.

In the case where one π^0 goes backward and the other goes forward with the neutron about 1% of the events would not trigger the A counter. This possible source of contamination was checked by doubling the thickness of lead in the A counter, which should reduce the percentage of undetected π^0's from 1.0% to 0.012%. After correcting for the change in neutron interactions in the A counter, there was no change in the counting rate within 10% statistical uncertainty.

IV. DISCUSSION OF RESULTS

A. Differential Cross Sections

Table II and Fig. 20 give the differential cross section at 180° calculated from our data with neutron coincidence required. The uncertainties are those discussed in Sec. III C, not including the 10% over-all systematic uncertainty. In Table II the differential cross sections with respect to u, $(d\sigma/du)$, are given as well as those with respect to $2\pi\cos\theta$, $(d\sigma/d\Omega)_{\text{c.m.}}$. The average value of the cosine of the center of mass angle, $(\cos\theta_{\text{c.m.}})_{\text{av}}$ (see Sec. III B) and the corresponding value of u, (u_{av}), are given as well as the interval in u, (δu), corresponding to the interval in $\cos\theta$ $[\delta\cos\theta = |-1.0000 - (\cos\theta_{\text{c.m.}})_{\text{av}}|]$.

In Fig. 20 these differential cross sections are plotted as a function of π^- momentum. They are seen to display a well defined structure below 4 GeV/c. There is a minimum at 2.1 GeV/c which may correspond to the 2190 MeV $T = \frac{1}{2}$ resonance. However, this minimum also corresponds kinematically to the dip observed in charge exchange cross sections to $t = -3$ (GeV/c)^2. There is no evidence for the 2650 MeV, $T = \frac{1}{2}$ resonance at 3.25 GeV/c. The maxima at 2.64 and 3.85 GeV/c correspond to the 2420 and 2850 MeV, $T = \frac{3}{2}$ resonances, but there is no evidence of a maximum at ~5.1 GeV/c such as that observed in $\pi^- p$ elastic scattering data.[18] In fact, above 4 GeV/c the differential cross section decreases smoothly within the uncertainties. We fitted an exponential

$$\frac{d\sigma}{d\Omega} = Ae^{-bp}$$

TABLE II. Center-of-mass differential cross sections for $\pi^- p \to \pi^0 n$ at 180° as a function of π^- momentum. $(\cos\theta_{c.m.})_{av}$ is the weighted average of the cosines of the angles included by each measurement. u_{av} corresponds to $(\cos\theta_{c.m.})_{av}$ and δu to the range in u which is included. The uncertainties given for $[(d\sigma/d\Omega)\ (180°)]_{c.m.}$ and $d\sigma/du\ (180°)$ are statistical only.

$(P_{lab})_{\pi^-}$ (GeV/c)	$(\cos\theta_{c.m.})_{av}$	$\left(\frac{d\sigma}{d\Omega}(180°)\right)_{c.m.}$ (μb/sr)	u_{av} [(GeV/c)^2]	δu [(GeV/c)^2]	$\frac{d\sigma}{du}(180°)$ [μb/(GeV/c)^2]
1.8	−0.9953	102.0 ± 4.2	0.1674	0.0062	481.8 ± 20
1.9	−0.9954	73.4 ± 3.5	0.1598	0.0065	324.7 ± 15
2.0	−0.9954	45.8 ± 2.4	0.1527	0.0070	190.5 ± 6.7
2.05	−0.9954	38.8 ± 2.5	0.1494	0.0072	156.7 ± 6.7
2.1	−0.9955	36.6 ± 3.2	0.1463	0.0072	143.6 ± 6.2
2.15	−0.9955	41.2 ± 2.7	0.1432	0.0074	157.2 ± 7.2
2.2	−0.9955	45.9 ± 2.2	0.1402	0.0076	170.5 ± 8.2
2.25	−0.9956	57.8 ± 2.4	0.1374	0.0076	209.0 ± 8.5
2.3	−0.9956	53.7 ± 2.3	0.1346	0.0078	189.3 ± 8.0
2.35	−0.9956	67.5 ± 2.8	0.1319	0.0080	232.0 ± 9.6
2.4	−0.9956	72.4 ± 2.4	0.1293	0.0082	242.8 ± 8.0
2.5	−0.9957	75.2 ± 2.0	0.1245	0.0084	240.4 ± 6.3
2.6	−0.9958	72.2 ± 2.0	0.1200	0.0086	220.6 ± 6.0
2.7	−0.9958	68.6 ± 2.9	0.1156	0.0090	200.6 ± 8.5
2.75	−0.9958	65.3 ± 2.7	0.1135	0.0092	187.0 ± 7.8
2.8	−0.9959	57.7 ± 2.5	0.1116	0.0092	161.8 ± 6.9
2.9	−0.9959	50.1 ± 2.1	0.1077	0.0096	135.0 ± 5.7
2.95	−0.9959	48.7 ± 2.6	0.1060	0.0096	128.7 ± 6.8
3.0	−0.9960	42.1 ± 1.2	0.1042	0.0097	109.1 ± 3.2
3.05	−0.9960	40.5 ± 1.7	0.1024	0.0099	103.0 ± 4.3
3.1	−0.9960	34.5 ± 1.6	0.1006	0.0101	86.1 ± 3.9
3.2	−0.9961	29.6 ± 1.4	0.0975	0.0102	71.3 ± 3.4
3.3	−0.9961	28.3 ± 1.3	0.0943	0.0105	65.8 ± 3.0
3.4	−0.9962	24.0 ± 1.2	0.0916	0.0106	54.0 ± 2.6
3.5	−0.9962	23.2 ± 1.0	0.0886	0.0110	50.5 ± 2.2
3.6	−0.9962	23.6 ± 1.1	0.0858	0.0113	49.8 ± 2.3
3.7	−0.9963	22.8 ± 1.1	0.0835	0.0114	46.6 ± 2.2
3.75	−0.9963	23.7 ± 1.0	0.0822	0.0115	47.8 ± 2.0
3.8	−0.9963	23.4 ± 1.1	0.0809	0.0117	46.5 ± 2.1
3.85	−0.9964	24.0 ± 1.1	0.0800	0.0116	47.0 ± 2.1
3.9	−0.9964	22.6 ± 1.2	0.0788	0.0117	43.6 ± 2.2
3.95	−0.9964	22.3 ± 1.2	0.0775	0.0119	42.4 ± 2.3
4.0	−0.9964	21.0 ± 1.2	0.0764	0.0121	39.4 ± 2.3
4.125	−0.9965	17.2 ± 1.0	0.0739	0.0121	31.2 ± 1.8
4.25	−0.9965	18.0 ± 0.9	0.0713	0.0125	31.6 ± 1.5
4.375	−0.9966	16.9 ± 0.9	0.0691	0.0126	28.7 ± 1.5
4.5	−0.9966	16.3 ± 0.8	0.0667	0.0130	26.9 ± 1.4
4.625	−0.9967	14.8 ± 0.8	0.0647	0.0130	23.7 ± 1.2
4.75	−0.9967	15.3 ± 0.9	0.0625	0.0134	23.8 ± 1.4
4.875	−0.9968	14.2 ± 0.9	0.0607	0.0133	21.4 ± 1.4
5.0	−0.9968	12.6 ± 1.0	0.0587	0.0137	18.5 ± 1.4
5.1	−0.9969	12.8 ± 0.7	0.0575	0.0136	18.4 ± 1.0
5.15	−0.9969	12.7 ± 0.7	0.0567	0.0137	18.1 ± 1.0
5.2	−0.9969	13.8 ± 0.7	0.0560	0.0138	19.4 ± 1.0
5.25	−0.9969	12.0 ± 0.7	0.0552	0.0140	16.7 ± 1.0
5.3	−0.9970	12.4 ± 0.7	0.0549	0.0137	17.1 ± 0.9
5.4	−0.9970	11.0 ± 0.6	0.0535	0.0140	14.9 ± 0.8
5.5	−0.9970	10.1 ± 1.1	0.0521	0.0142	13.4 ± 1.4
5.625	−0.9971	10.8 ± 1.0	0.0509	0.0141	14.0 ± 1.3
5.75	−0.9971	10.3 ± 1.0	0.0492	0.0144	13.0 ± 1.3
5.875	−0.9972	10.1 ± 0.9	0.0481	0.0143	12.5 ± 1.2
6.0	−0.9972	9.1 ± 0.7	0.0466	0.0146	11.0 ± 0.8

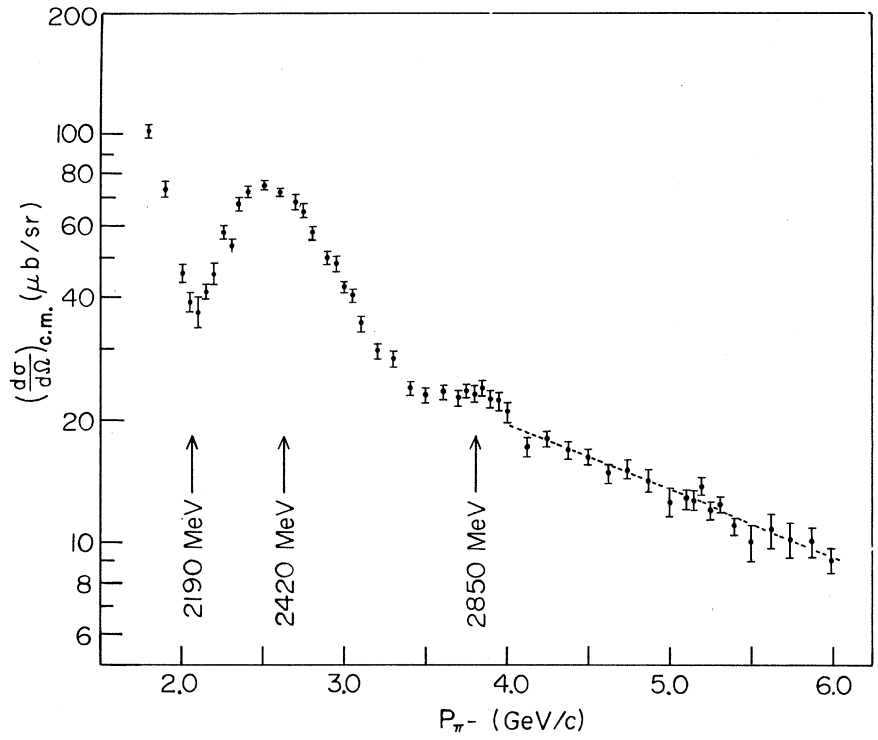

FIG. 20. Center-of-mass differential cross section $\pi^- p \to \pi^0 n$ at 180° as a function of π^- momentum. The line is the best fit of an exponential to the data between 4 and 6 GeV/c [$(d\sigma/d\Omega) = A e^{-bp}$, $A = 85.2 \pm 2.1$ μb/sr, $b = 0.36 \pm 0.025$ (GeV/c)$^{-1}$]. The π^- momenta corresponding to the $T = \frac{1}{2}$, 2190 MeV, and the $T = \frac{3}{2}$, 2420 and 2850 MeV, resonances are indicated.

to our values from 4 to 6 GeV/c inclusive and obtained $A = 85.2 \pm 2.1$ μb/sr, $b = 0.368 \pm 0.025$ (GeV/c)$^{-1}$ with $\chi^2 = 11$ for 20 points or confidence level ~100%. This exponential fit is shown by the dashed line in Fig. 20. (These data can also be fit by p^{-n} with $n = 1.86 \pm 0.15$, $\chi^2 = 12$.)

In Fig. 21 we present a compilation of results from other experiments for the differential cross section for the charge-exchange reaction at angles close to 180° together with the results of this experiment. Within the rather large uncertainties the lower momentum data of Bulos *et al.*[1] connect smoothly with that of Crouch *et al.*[2] which are in agreement with these data in the region where they overlap. The values of Antopolsky *et al.*[3] agree within their large uncertainties with the data of Bulos, Crouch, and this experiment except for their point at 2.6 GeV/c which is nearly 7 standard deviations below our value. At 4.0 GeV/c the differential cross sections of Schneider *et al.*[4] are plotted both for $\cos\theta = -0.999$ and $\cos\theta = -0.996$. The value for $\cos\theta = -0.999$ is within 1 standard deviation of our value, while that for $\cos\theta = -0.996$ agrees excellently. This is what would be expected since our effective angle corresponds to $\cos\theta_{av} = -0.9964$. At 6 GeV/$c$ the value of Schneider *et al.* for $\cos\theta = -0.999$ is 1 standard deviation above our value and that for $\cos\theta_{av} = -0.9972$ is 2 standard deviations below. At 6.0 GeV/c there is also given the value for the differential cross section extrapolated to 180° of Boright *et al.*,[5] which agrees excellently with the value of Schneider *et al.* at $\cos\theta = -0.999$. Also shown is the extrapolation to higher momenta of the exponential fit to our data. This agrees with the 8-GeV/c point of Schneider *et al.* and is 1.3 standard deviations below their 11-GeV/c point. The values of Chase *et al.*[6] are significantly below our data at all momenta. At 2 GeV/c their value is 0.34 of ours; the data of Crouch *et al.* and Antopolsky *et al.* do not contain 2-GeV/c points but indicate values in agreement with ours. At 3 GeV/c the differential cross sections of Chase *et al.* is 0.47 the value of ours and 2 standard deviations below the value of Antopolsky *et al.* At 4 GeV/c the value of Chase *et al.* is 0.40 that of ours and 1.3 standard deviations below the value of Schneider *et al.* at $\cos\theta = -0.996$ to which it corresponds in angle. At 6 GeV/c the value of Chase *et al.* is 0.64 that of ours and 1.1 standard deviations below the value of Schneider *et al.* at $\cos\theta = -0.995$ to which it corresponds in angle. From the internal consistency of our data, espe-

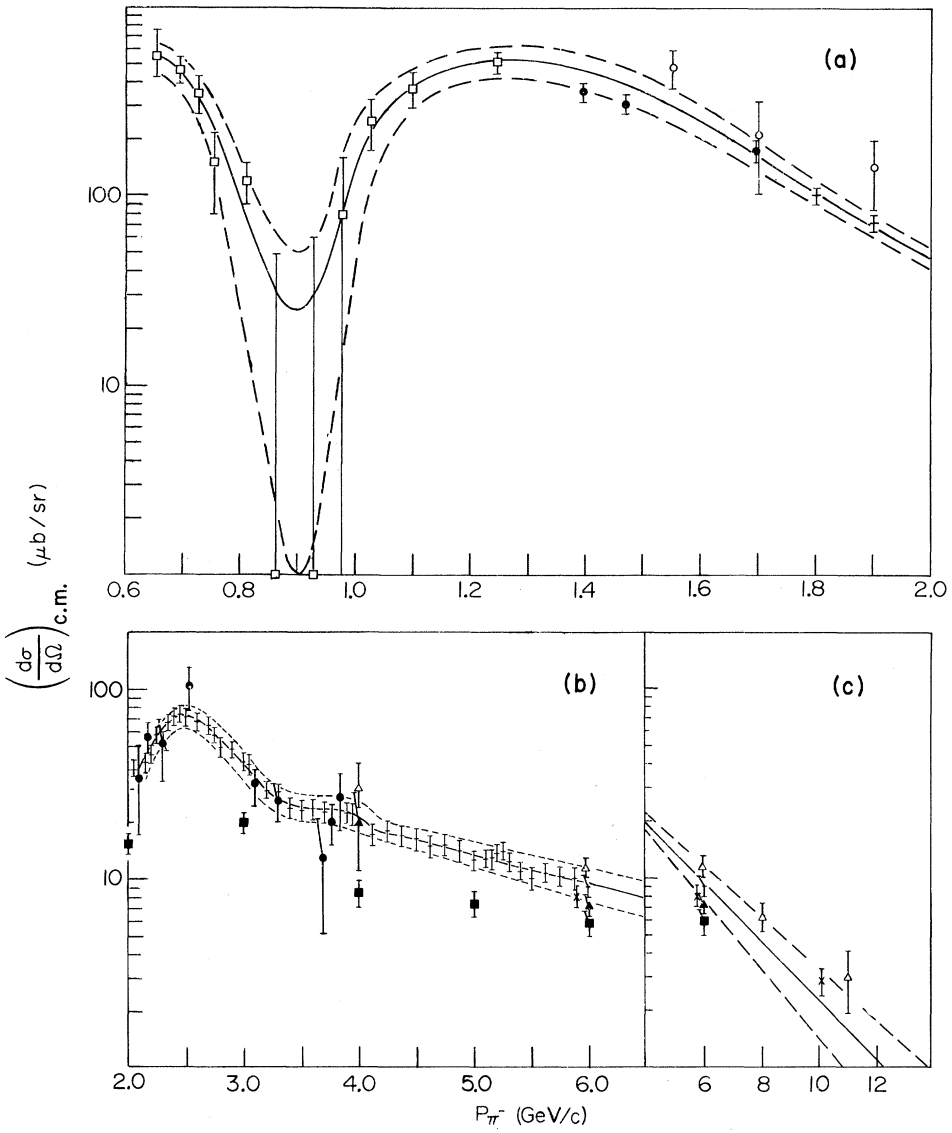

FIG. 21. Compilation of data on the differential cross sections for $\pi^- p \to \pi^0 n$ at 180°. □ Bulos *et al.* (Ref. 1), ● Crouch *et al.* (Ref. 17), ○ Antopolsky *et al.* (Ref. 3), † this experiment, ■ Chase *et al.* (Ref. 6), × Boright *et al.* (Ref. 5), △ Schneider *et al.* (Ref. 4), at $\cos\theta \lesssim -0.998$, ▲ Schneider *et al.* (Ref. 4), at $-0.998 < \cos\theta \lesssim -0.995$.

cially the agreement of our cross sections where neutron is required with those where neutron is not required, we conclude that our data are reliable. The results of our experimental determination of neutron counter efficiency (see Sec. II D) are in disagreement with the efficiencies quoted by Chase *et al.* for their detector. This may explain part of the discrepancy between their results and the results of the other experiments cited above.

B. Comparison with a Dual-Resonance Model

Figure 22 again shows our differential cross sections plotted as a function of π^- momentum and a curve which is the best fit to our data of a modification of a dual-resonance model[8] in which the πN amplitudes are a linear combination of Veneziano terms,[9] one term for each pair of Regge trajectories allowed in the s, t, and u channels. The modification is introduced to allow for finite width resonances and is achieved by phenomenologically introducing in all the Regge trajectories a common linear imaginary part. This is suggested by the observed mass dependence of the widths of the baryon resonances lying on the N_α, N_γ, and Δ_δ trajectories. The πN invariant amplitudes, A_ρ and B_ρ, corresponding to ρ exchange in the t channel, are thus

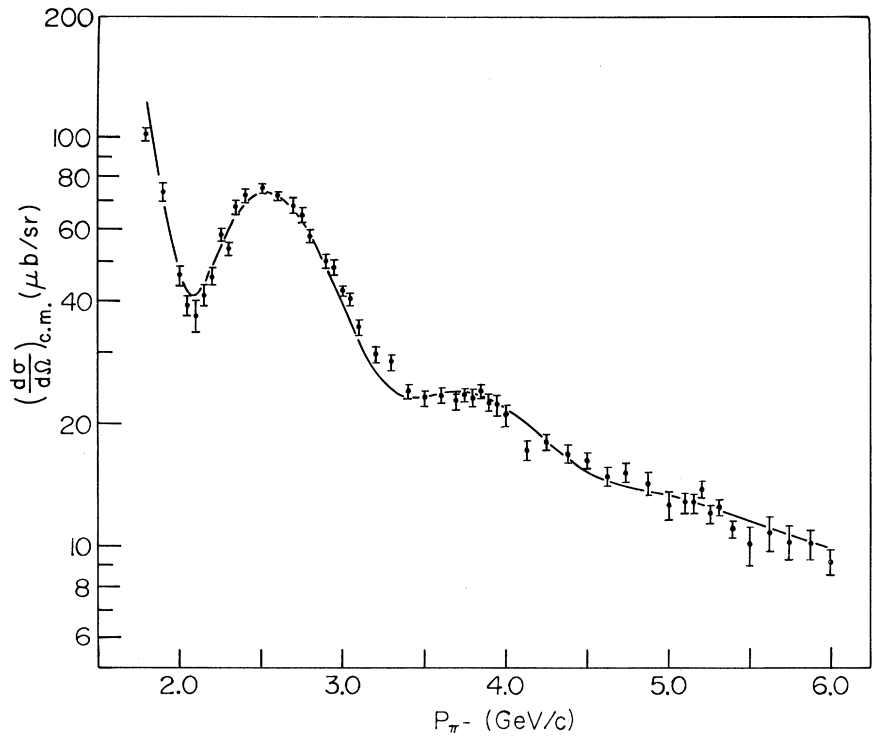

FIG. 22. Center-of-mass differential cross section for $\pi^- p \to \pi^0 n$ at 180°. The data of this experiment are fit by the prediction of a modified dual-resonance model containing five parameters.

$$A_\rho(s,t,u)=\frac{\beta_\rho^{(1)}}{\pi}\left[\sum_F b_F C^-\langle 1-\alpha_\rho(t),\tfrac{3}{2}-\alpha_F(s)\rangle + pC^-\langle \tfrac{3}{2}-\alpha_{N_\alpha}(s),\tfrac{3}{2}-\alpha_{\Delta_\delta}(u)\rangle + (1-p)C^-\langle \tfrac{3}{2}-\alpha_{N_\alpha}(s),\tfrac{3}{2}-\alpha_{N_\gamma}(u)\rangle\right], \tag{12}$$

$$B_\rho(s,t,u)=\frac{\beta^{(2)}P'}{\pi}\left\{\sum_F b'_F\left[B^+\langle 1-\alpha_\rho(t),\tfrac{1}{2}-\alpha_F(s)\rangle + S_F\langle \tfrac{1}{2}-\alpha_F(s),\tfrac{1}{2}-\alpha_F(u)\rangle\right]\right\}, \tag{13}$$

where

$$B(x,y)=\Gamma(x)\Gamma(y)/\Gamma(x+y), \tag{14}$$

$$C(x,y)=\Gamma(x)\Gamma(y)/\Gamma(x+y-1), \tag{15}$$

$$b_{N_\alpha}=1,\quad b_{\Delta_\delta}=p,\quad b_{N_\gamma}=1-p,$$
$$b'_{N_\alpha}=1,\quad b'_{\Delta_\delta}=-\tfrac{1}{2}p',\quad b'_{N_\gamma}=1-p',$$
$$S_{N_\alpha}=1,\quad S_{\Delta_\delta}=-1,\quad S_{N_\gamma}=-1;$$

the sums $\sum_F$ run over the fermion trajectories N_α, Δ_δ, and N_γ and the superscripts + (−) mean symmetric (antisymmetric) with respect to s-u crossing. In this model the Regge trajectories have the form

$$\alpha(s)=\alpha_0+\alpha_1 s+i\beta s. \tag{16}$$

In addition to the four parameters $\beta_\rho^{(1)}$, $\beta_P^{(2)}$, p, and p' of the original Igi[8] amplitudes, we have introduced here the slope β of the imaginary part of the trajectories as fifth parameter of the model.

Igi's model[8] has no mechanism for avoiding parity doubling; it also ignores all terms that do not contribute to the leading order in the asymptotic region, terms that could be of importance in the energy range considered here. (The Pomeranchuk trajectory is not included in the model either, but this is unimportant for the reaction under consideration.) Despite these shortcomings, we choose to work with the Igi expressions for the πN amplitudes because of their relative simplicity.

The solid line in Fig. 22 is the result of a minimum χ^2 fit to our data of the model described above, which contains five adjustable parameters. The real, linear parts of the trajectories are assumed to be parallel, with a common slope equal to 0.86 GeV^{-2} and intercepts equal to 0.5, −0.256, −0.55, and 0.18 for the ρ, N_α, N_γ, and Δ_δ trajectories, respectively. The best fit had a $\chi^2=79$ for 52 points for the following values of the parameters:

$$\beta=0.23\ \text{GeV}^{-2},$$

$\beta_\rho^{(1)} = 19.84$ mb GeV,

$\beta_P^{(2)} = 7.91$ mb,

$p = 0.38$,

$p' = -0.082$.

(The point at 1.8 GeV/c contributes $\chi^2 = 21$; excluding this, the confidence level is 15%.) The value of β is about twice the value obtained from the experimental resonance widths. This could be due to wrong parametrization of the imaginary part of the trajectories in the unphysical region. In fact, it would be naive to assume that the effect of cuts in the Regge trajectories along the negative axis are well approximated by a linear imaginary part, as is implied here implicitly by the form of the trajectories. Ignoring the cuts altogether by assuming the trajectories to be real below threshold leads to a significantly poorer fit to the backward charge exchange data. Other forms for the trajectories were also investigated, e.g., (a) nonparallel, linear real parts with slopes and intercepts provided for the baryons by their Chew-Frautschi plots, and (b) square-root dependence of the imaginary part above threshold; none of these forms was able to fit the data as well as the one we assumed above.

The values of the remaining four parameters are quite different from the ones obtained by Igi from the asymptotic limit of his model. The comparison is not very meaningful, however, since the amplitudes employed here have complex parts, whereas Igi's amplitudes are essentially real.

The surprisingly good quality of the fit of this model to data of such high statistical accuracy and extending over a range of momenta that includes both high and intermediate regions, encourages the idea that phenomenological modifications of models based on Veneziano's formula may be useful in describing experiments.

C. πN Amplitudes

The s- and u-channel amplitudes for $\pi^+ p$ elastic scattering (A), $\pi^- p$ elastic scattering (A^-), and $\pi^- p$ charge exchange (A^0) are related to the corresponding πN isotopic-spin amplitudes ($A_{1/2}$ and $A_{3/2}$) as follows.

s channel:

$$\begin{aligned} A^+ &= \langle \pi^+ p | A | \pi^+ p \rangle = A_{3/2}, \\ A^- &= \langle \pi^- p | A | \pi^- p \rangle = \tfrac{2}{3} A_{1/2} + \tfrac{1}{3} A_{3/2}, \\ A^0 &= \langle \pi^0 n | A | \pi^- p \rangle = \frac{\sqrt{2}}{3} A_{3/2} - \frac{\sqrt{2}}{3} A_{1/2}. \end{aligned} \tag{17}$$

u channel:

$$\begin{aligned} A^+ &= \langle \pi^- p | A | \pi^- p \rangle = \tfrac{2}{3} A_{1/2} + \tfrac{1}{3} A_{3/2}, \\ A^- &= \langle \pi^+ p | A | \pi^+ p \rangle = A_{3/2}, \\ A^0 &= \langle \pi^0 p | A | \pi^+ n \rangle = \frac{\sqrt{2}}{3} A_{3/2} - \frac{\sqrt{2}}{3} A_{1/2}. \end{aligned} \tag{18}$$

Thus, one can calculate $|A_{1/2}|$, $|A_{3/2}|$, and the absolute value of their relative phase $|\delta|$ from the $\pi^+ p$ elastic (σ^+), the π^- elastic (σ^-), and charge-exchange (σ^0) differential cross sections at 180°. The u-channel relations are

$$\begin{aligned} |A_{3/2}| &= (\sigma^-)^{1/2}, \\ |A_{1/2}| &= [\tfrac{3}{2}(\sigma^0 + \sigma^+ - \tfrac{1}{3}\sigma^-)]^{1/2}, \\ \cos\delta &= \frac{3}{4}\left(\frac{\sigma^+ - 2\sigma^0}{\sigma^-} + \frac{1}{3}\right)\frac{|A_{3/2}|}{|A_{1/2}|}. \end{aligned} \tag{19}$$

The s-channel relations are obtained by interchanging σ^+ and σ^- in these equations.

Figures 23 and 24 show the compilations that were made of $\pi^+ p$ elastic[19-32] and $\pi^- p$ elastic[18,24-34] scattering differential cross sections at ~180°. The compilation of the π^- charge-exchange differential cross sections in Fig. 19 has already been discussed. Only data were included for which $\cos\theta < -0.99$ or which were extrapolated to 180°. The uncertainties include systematic uncertainties wherever they were available, as well as statistical or extrapolation uncertainties. The solid lines indicate the values actually used in calculating the amplitudes and the dashed lines the uncertainty limits. Above the region of structure these lines were the result of a fit of an exponential to that data, $d\sigma/d\Omega = Ae^{-bp}$. The fit for the charge exchange data has already been discussed (Sec. IV A). The $\pi^+ p$ data were fitted above 5.5 GeV/c by $A = 93 \pm 7$ μb/sr, $b = 0.183 \pm 0.012$ (GeV/c)$^{-1}$ with $\chi^2 = 30$ for 8 points. The $\pi^- p$ elastic data was fit above 5.5 GeV/c by $A = 10.05 \pm 0.95$ μb/sr, $b = 0.120 \pm 0.010$ (GeV/c)$^{-1}$ with $\chi^2 = 13$ for 11 points.

The s-channel values calculated for $|A_{3/2}|$, $|A_{1/2}|$, and $\cos\delta$ are given in Fig. 25 as a function of $\sqrt{s}$. The dots indicate the results of the calculation using the central values of the cross sections and the bars indicate the uncertainty due to the uncertainty limits of the cross sections. In the region $\sqrt{s} < 2$ GeV/c, the central values of the cross sections gave nonphysical values for $|A_{1/2}|$ ($|A_{1/2}|^2 < 0$) and $\cos\delta$ ($\cos^2\delta > 1$). However, some combinations of the uncertainty limits and central values gave physical values for $|A_{1/2}|$ and $\cos\delta$ and these are indicated by ×'s. This indicates that there are inconsistencies in the data in this region ($p_\pi < 1.8$ GeV/c) and the values should be checked experimentally. For $\sqrt{s} > 4.3$ GeV/c, $\cos\delta > 1$ for the central values of the cross sections, although the uncertainty spans the full region of possible values

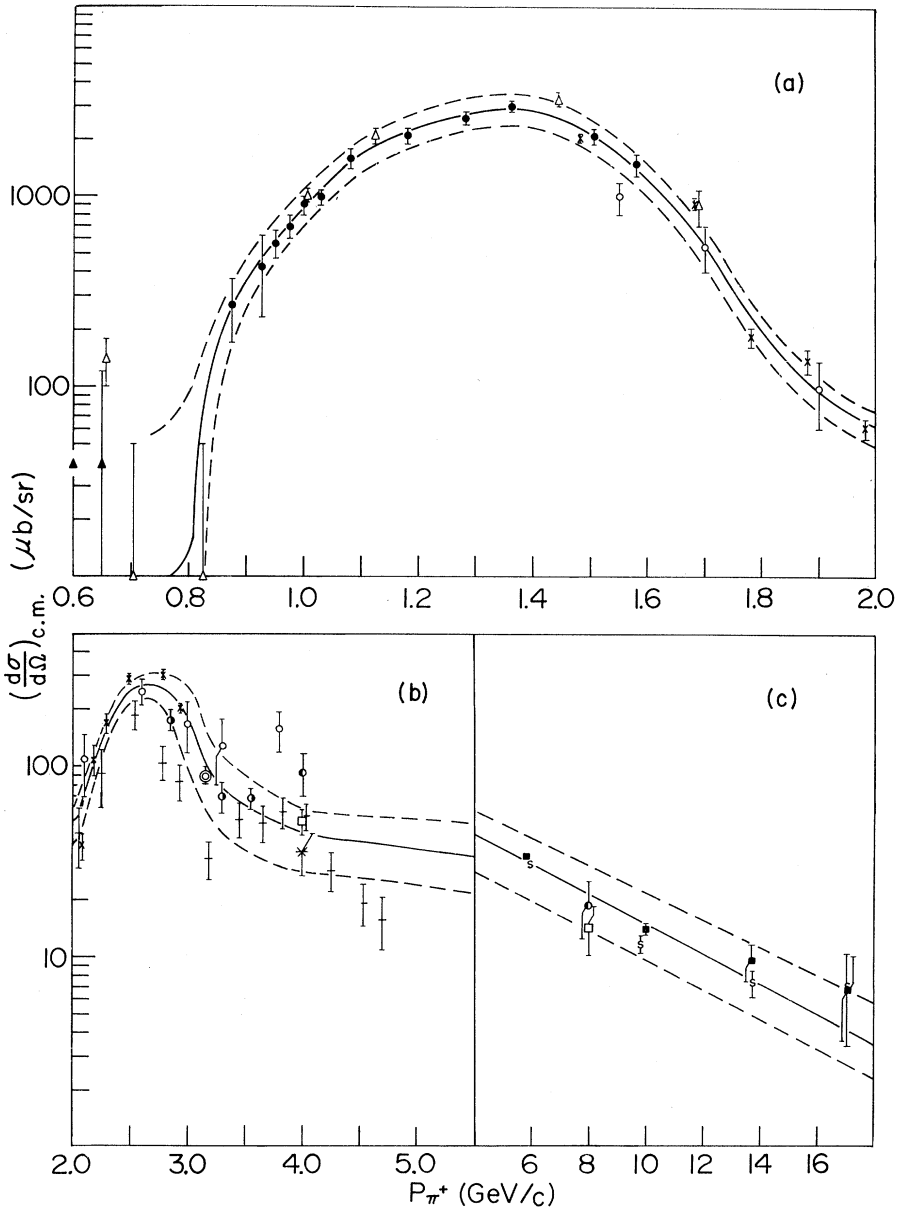

FIG. 23. Compilation of data on the differential cross sections for $\pi^+p \to \pi^+p$ at 180°. ▲ Ogden *et al.* (Ref. 29), △ Helland *et al.* (Ref. 30), ● Duke *et al.* (Ref. 25), ○ Antopolsky *et al.* (Ref. 23), × Carroll *et al.* (Ref. 19), ■ Ashmore *et al.* (Ref. 26), □ Frisken *et al.* (Ref. 27), ◐ Orear *et al.* (Ref. 28), ◑ Baker *et al.* (Ref. 24), † Dobrowolski *et al.* (Ref. 20), ◎ Savin *et al.* (Ref. 21), * Aachen *et al.* (Ref. 22), s Owen *et al.* (Ref. 31).

of cosδ. This reflects the sparseness of the cross-section data in this region and the corresponding uncertainties of the exponential fits.

The data for $|A_{3/2}|$ are what would be expected from the known $T=\frac{3}{2}$ resonances with peaks at ~1.8 GeV/c and ~2.4 GeV/c corresponding to the 1630- to 1940-MeV and the 2420-MeV δ's. These peaks are separated by a dip with a minimum at about 2.2 GeV/c. The curve was calculated from the parameters for the fit of the dual-resonance model (Sec. IV B) to the charge-exchange cross section. It does not reproduce the maxima and minima, but approximates the results for $\sqrt{s} > 2.5$ GeV/c.

The data for $|A_{1/2}|$ are consistent with the $T=\frac{1}{2}$ resonances between 1470 and 1860 MeV. However, the dip which would be expected between 1.9 and 2.2 GeV/c, corresponding to the break between this first group of resonances and the 2190- and 2220-MeV resonances, is high, ~2.2 GeV/c. There are second and third maxima, but they are at 2.4

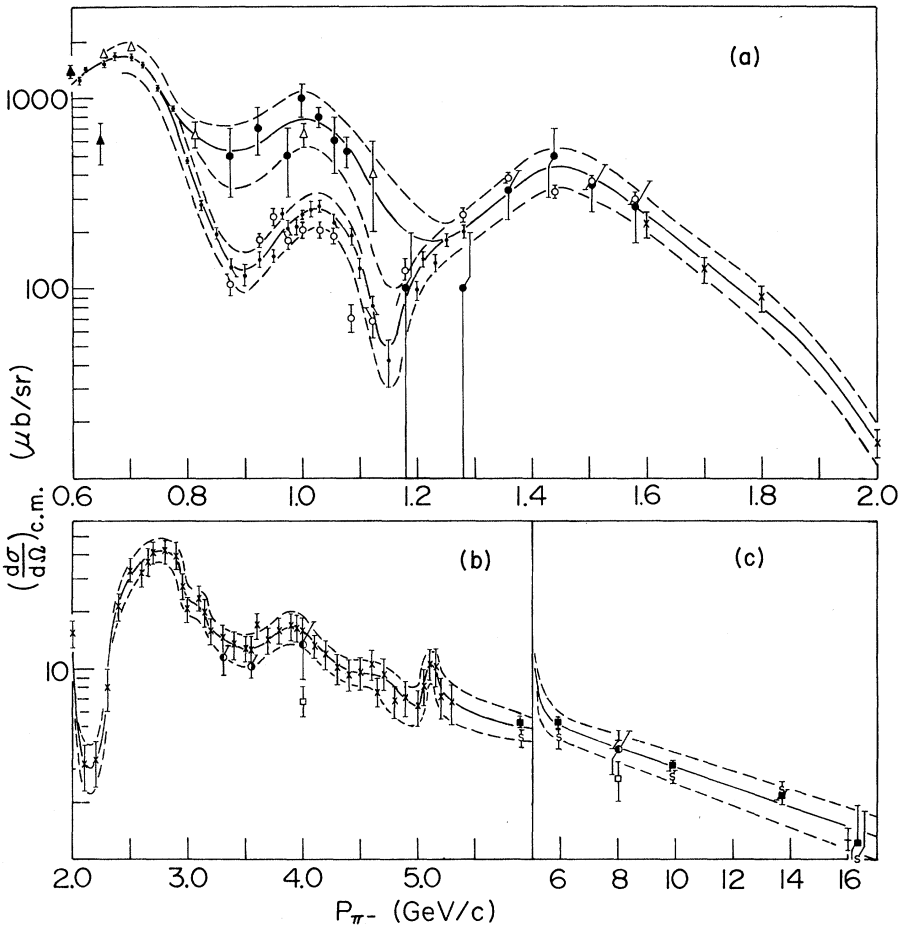

FIG. 24. Compilation of data on the differential cross sections for $\pi^- p \to \pi^- p$ at 180°. ▲ Ogden *et al.* (Ref. 29), △ Helland *et al.* (Ref. 30), ● Duke *et al.* (Ref. 25), • Crabb *et al.* (Ref. 34), ○ Abillon *et al.* (Ref. 33), × Kormanyos *et al.* (Ref. 18), ■ Ashmore *et al.* (Ref. 26), □ Frisken *et al.* (Ref. 27), ◐ Orear *et al.* (Ref. 28), ◑ Baker *et al.* (Ref. 24), s Owen *et al.* (Ref. 31), † Anderson *et al.* (Ref. 32).

and 2.8 GeV/c rather than the expected 2190–2220 and 2650 MeV. The curve calculated from the dual-resonance model does not agree with the data but roughly reproduces its features for $\sqrt{s} < 2.8$ GeV/c. At higher values of $\sqrt{s}$, the calculated curve remains constant while the values from the data decrease.

The most striking feature of the data for $\cos\delta$ is the sharp minimum for $\sqrt{s} = 2.2$ GeV/c. This is not reproduced by the curve calculated from the dual-resonance model. In the region $2.5 < \sqrt{s} < 3.5$, $\cos\delta$ is constant at ~ -0.25 but then increases for larger values of $\sqrt{s}$.

Figure 26 gives the u-channel values for $|A_{3/2}|$, $|A_{1/2}|$, and $\cos\delta$. Again in the low-momentum region ($u > 0.54$ GeV/c) the central cross-section values give nonphysical values for $|A_{1/2}|$ and $\cos\delta$. It should be pointed out that the combinations of cross-section limits which give physical results for the u channel are not the same as those which do so for the s channel.

$|A_{3/2}|$, $|A_{1/2}|$, and $\cos\delta$ all display a marked structure. In particular, they all have a marked minimum at $\sqrt{u} \sim 0.4$ GeV/c, which corresponds to $\sqrt{s} \sim 2.2$ GeV/c, where dips were also observed in the s-channel data. As $\sqrt{u}$ becomes small, $\cos\delta$ increases from 0 to 1.0, and the central cross-section values give $\cos\delta > 1$ for the smallest values of u. This is in disagreement with the prediction of a constant value, $|\cos\delta| = 0.64$, by the Regge model, if only the nucleon and δ trajectories are considered.

V. CONCLUSIONS

The differential cross sections for pion charge-exchange reactions close to 180° measured in this experiment are in good agreement with the values obtained by other measurements except for those of Chase *et al.*[6] Our measurements of neutron

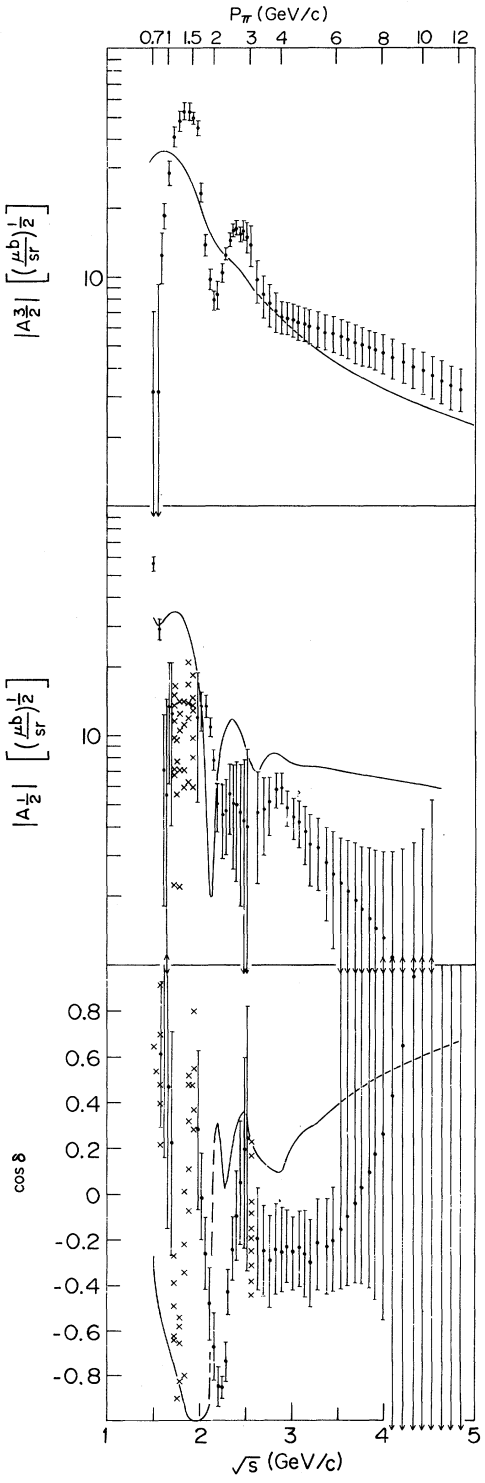

FIG. 25. Moduli of the s channel $T=\frac{1}{2}$ and $T=\frac{3}{2}$ amplitudes and the cosine of their relative phase as a function of $\sqrt{s}$ and of incident pion laboratory momentum. The curves are the predictions of the modified dual resonance model using the parameters from the fit to our charge-exchange data.

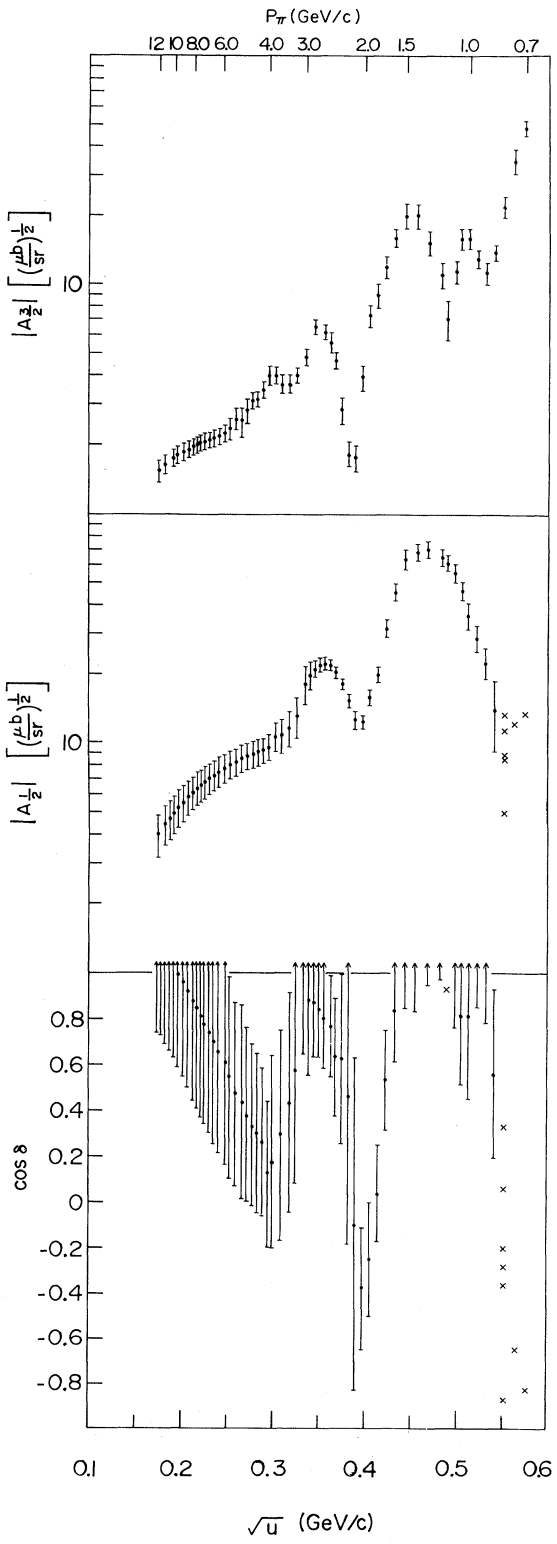

FIG. 26. Moduli of the u channel $T=\frac{1}{2}$ and $T=\frac{3}{2}$ amplitudes and the cosine of their relative phase as a function of $\sqrt{u_x}$ and of incident pion laboratory momentum.

counter efficiency lead us to believe that at least part of the difference may be due to an incorrect estimate in their experiment of the neutron counter efficiency which did not take into account sizeable edge losses.

Our data were well fitted by a curve calculated from a dual-resonance model. In the region from 4 to 6 GeV/c they were also fitted by an exponential.

From a compilation of data on elastic $\pi^{\pm} p$ scattering and $\pi^- p$ charge-exchange scattering, $|A_{3/2}|$, $|A_{1/2}|$, and $\cos\delta$ could be calculated in both the s and the u channel. The results of this analysis were not satisfactory since, in several regions, the data yielded nonphysical values. These are most probably due to systematic differences between the various experiments. The s-channel values varied with $\sqrt{s}$ as would be expected on the basis of the known resonances, except that there appeared to be a decrease in $|A_{1/2}|$ at 2.2 GeV/c rather than the maximum expected from the 2190-MeV resonance. There was a marked minimum at 2.2 GeV/c in $|A_{3/2}|$ and $\cos\delta$ and also in the u-channel values for $|A_{3/2}|$, $|A_{1/2}|$, and $\cos\delta$ at the corresponding value $\sqrt{u}$ = 0.4 GeV/c. The parameters from the fit of the dual model to the charge-exchange data did not give curves for $|A_{3/2}|$, $|A_{1/2}|$, and $\cos\delta$ in good agreement with the values obtained. The u-channel $|\cos\delta|$ did not approach a constant value at high momentum (low $\sqrt{u}$) as predicted by a simple Regge-pole model.

ACKNOWLEDGMENTS

We thank the staff of the AD and HEF Divisions of ANL for their invaluable assistance, without which this experiment would not have been possible.

---

*Present address: Département de Physique des Particules Elémentaires, CEN, Saclay, France.

‡Present address: Massachusetts Institute of Technology, Cambridge, Mass.

§Permanent address: Massachusetts Institute of Technology, Cambridge, Mass.

†This work is supported in part through funds provided by the U. S. Atomic Energy Commission under Contract No. AT(11-1)3069.

[1]F. Bulos *et al.*, Phys. Rev. Letters 13, 558 (1964).

[2]H. R. Crouch *et al.*, Phys. Rev. Letters 21, 849 (1968).

[3]V. D. Antopolsky *et al.*, Phys. Letters 28B, 223 (1968).

[4]J. Schneider *et al.*, Phys. Rev. Letters 23, 1068 (1969).

[5]J. P. Boright *et al.*, Phys. Letters 33B, 615 (1970).

[6]R. C. Chase *et al.*, Phys. Rev. D 2, 2588 (1970).

[7]V. Kistiakowsky *et al.*, Phys. Rev. Letters 22, 618 (1969); 26, 1498 (1971).

[8]K. Igi, Phys. Letters 28B, 330 (1968).

[9]G. Veneziano, Nuovo Cimento 57A, 190 (1968).

[10]L. G. Ratner, Argonne National Laboratory internal report (unpublished).

[11]The bending magnets are 18 in. wide by 6 in. high by 72 in. long. The quadrupole magnets are 10 in. nominal diameter and 36 in. long.

[12]Radiation length: lead, 0.58 cm; iron, 1.8 cm; scintillator, 48 cm. Conversion length = $\frac{7}{9}$ radiation length, used in general arguments. Conversion length = (radiation length)/D, where $D = -0.42 + 0.309\ (\ln P_\gamma) - 0.0201\ (\ln P_\gamma)^2$, used in Monte Carlo calculations [see B. Rossi, *High Energy Particles* (Prentice-Hall, New York, 1952)].

[13]RCA 8575.

[14]John H. Atkinson *et al.*, Phys. Rev. 123, 1850 (1961). The total pion inelastic cross section for lead given in this reference is 1670 mb. We used a reaction length for lead equivalent to this, 18.2 cm. The reaction length used for iron, 16.8 cm, was based on this and the total cross sections given in Particle Data Group, Rev. Mod. Phys. 43, S1 (1971).

[15]The detailed calculation is available from the authors as an unpublished appendix.

[16]The total interaction length for scintillator, 55.5 cm, from Particle Data Group, Rev. Mod. Phys. 43, S1 (1971). The scintillator is NE 102.

[17]H. R. Crouch *et al.*, unpublished results.

[18]S. W. Kormanyos *et al.*, Phys. Rev. Letters 16, 709 (1966); Phys. Rev. 164, 1661 (1967).

[19]A. S. Carroll *et al.*, Phys. Rev. Letters 20, 607 (1968).

[20]T. Dobrowolski *et al.*, Phys. Letters 24B, 203 (1967).

[21]I. A. Savin *et al.*, Phys. Letters 17, 68 (1965).

[22]Aachen-Berlin-Birmingham-Bonn-Hamburg-London (I.C.)-Munchen Collaboration, Phys. Letters 10, 248 (1964).

[23]V. D. Antopolsky *et al.*, Phys. Letters 28B, 220 (1968).

[24]W. F. Baker *et al.*, Phys. Letters 23, 605 (1966); 25B, 361 (1967).

[25]P. J. Duke *et al.*, Phys. Rev. 149, 1077 (1966).

[26]A. Ashmore *et al.*, Phys. Rev. Letters 19, 460 (1967).

[27]W. R. Frisken *et al.*, Phys. Rev. Letters 15, 313 (1965).

[28]J. Orear *et al.*, Phys. Rev. 152, 1162 (1966).

[29]P. M. Ogden *et al.*, Phys. Rev. 137, B1115 (1965).

[30]J. A. Helland *et al.*, Phys. Rev. 134, B1062 (1964); 134, B1079 (1964).

[31]D. P. Owen *et al.*, Phys. Rev. 181, 1794 (1969).

[32]E. W. Anderson *et al.*, Phys. Rev. Letters 20, 1529 (1968).

[33]J. M. Abillon *et al.*, Phys. Letters 32B, 712 (1970).

[34]D. G. Crabb *et al.*, Phys. Rev. Letters 27, 216 (1971).